NKS-511
ISBN 978-87-7893-610-3

Low temperature crack propagation in nuclear shut-down water chemistry of Alloy 52 with potential effects of hydrogen

Zaiqing Que[1], Pedro A. Ferreiros[1], Yanling Ge[1]

Sebastian Lindqvist[1], Timo Veijola[1], Mattias Thuvander[2]

Björn Forssgren[3], Mimmi Bäck[4], Pål Efsing [3, 5]

[1] VTT Technical Research Centre of Finland, 02130 Espoo, Finland
[2] Chalmers University of Technology, Department of Physics, SE-412 96, Göteborg, Sweden
[3] Ringhals AB, SE-43285 Väröbacka, Sweden
[4] OKG AB, 57283 Oskarshamn, Sweden
[5] Department of Solid Mechanics, Royal Institute of Technology (KTH), SE-100 44 Stockholm, Sweden

February 2026

Abstract

Constant-displacement bolt-loaded compact tension specimens of Nickel-based Alloy 52 were exposed to boiling water reactor environment for 12 years and then in cold shutdown water environment for a further 3 years in a Swedish nuclear power plant at a stress intensity factor of 20 MPa√m. Follow decontamination and specimen opening, unexpected crack extensions of 3–4.5 mm were observed. The fracture surface and the cross-sectional deformation microstructure were examined by electron microscopies techniques up to nanoscale. The dominant fracture mode is transgranular along the close-packed {111} planes. Extensive shear bands were observed in vicinity of the crack tips, revealing localized plasticity. Hydrogen reduces stacking fault energy, results in localized plasticity and enhances shear bands formation. Low temperature crack propagation with evident effects of hydrogen was considered as the potential cause of the crack propagation in Alloy 52 without external dynamic loading in cold shut down water chemistry. The project promotes knowledge transfer, improves nuclear materials and fracture mechanics competence and strengthens the connections and experience exchange between the Nordic research organizations, universities, industries, authorities, and especially the young generation. The project deals with structural integrity, long-term operation, and ageing management, which are relevant for both present and future nuclear power plants. The technical results provide a basis for assessment of long-term operation for the Finnish and Swedish nuclear power plants for both the operators and the regulatory perspectives. Dissemination through the peer reviewed publications and the oral presentations at the international conferences ensured the knowledge exchange in international and Nordic networks.

Key words

Dissimilar metal weld, Alloy 52, fusion boundary, characterization, fracture mechanical test, hydrogen embrittlement; low temperature crack propagation

NKS-511
ISBN 978-87-7893-610-3
Electronic report, February 2026
NKS Secretariat
P.O. Box 49
DK - 4000 Roskilde, Denmark
Phone +45 4677 4041
www.nks.org
e-mail nks@nks.org

Low temperature crack propagation in nuclear shut-down water chemistry of Alloy 52 with potential effects of hydrogen

Final Report from the NKS-R FEMMA activity

(Contract: AFT/NKS-R(25)134/1)

Zaiqing Que[1], Pedro A. Ferreiros[1], Yanling Ge[1], Sebastian Lindqvist[1], Timo Veijola[1]
Mattias Thuvander[2]
Björn Forssgren[3]
Mimmi Bäck[4]
Pål Efsing[3, 5]

[1] VTT Technical Research Centre of Finland, 02130 Espoo, Finland
[2] Chalmers University of Technology, Department of Physics, SE-412 96, Göteborg, Sweden
[3] Ringhals AB, SE-43285 Väröbacka, Sweden
[4] OKG AB, 57283 Oskarshamn, Sweden
[5] Department of Solid Mechanics, Royal Institute of Technology (KTH), SE-100 44 Stockholm, Sweden

Table of contents

1. Introduction

Nickel-Chromium based alloys offer a good combination of corrosion resistance and ductility, with a thermal expansion coefficient in-line with the structural materials being welded. Nickel-based filler metals are routinely employed as weld materials in power generation systems to join bainitic/ferritic LAS reactor pressure vessel with austenitic stainless steel pipes. It can become a concern for the structural integrity in nuclear power systems, structures and components since several failures have been observed in such welds in nuclear power plants (NPPs). Moreover, Nickel-Chromium based welds have been suggested to be sensitive to a sub-critical brittle crack propagation in a low temperature aqueous environment termed low temperature crack propagation (LTCP). This problem can be of high relevance when a reactor goes through a shutdown phase or an extended outage.

Constant-displacement bolt-loaded compact tension specimens of Nickel-based Alloy 52 were exposed to boiling water reactor (BWR) environment for 12 years and then in cold shutdown water environment for a further 3 years in a Swedish nuclear power plant at a stress intensity factor of 20 MPa √ m. Follow decontamination and specimen opening, unexpected crack extensions of 3 – 4.5 mm were observed on the specimens. The fracture surface and the cross sectional deformation microstructure were analyzed at nanoscale with analytical electron microscopy to reveal the underlying cracking mechanisms. The intrinsic interactions of microstructure and hydrogen and the resulting localized deformation were discussed. The implications, relevance and precautions of LTCP for a reactor in a shutdown phase or an extended outage were addressed.

As a part of the NKS-R program in 2025, VTT, Chalmers University of Technology, Ringhals, OKG, and KTH have continued to study the microstructural properties and fracture mechanical performance of an Alloy 52 weld. The project deals with structural integrity, long-term operation, and ageing management, which are relevant for both present and future nuclear power plants. The technical results provide a basis for the assessment of long-term operation for the Finnish and Swedish nuclear power plants for both the operators and the regulatory perspectives.

There are active involvements of young scientists in NKS-FEMMA. The work is mainly executed by three PhD students Noora Hytönen, Laura Sirkiä and Timo Veijola. Young scientists or postdocs, David Mayweg, Armin Halilovic and Pedro Ferreiros are the main working group. A Master Thesis student Anni Li was hired at KTH. Additionally, young engineers and researchers at TVO, KTH, Forsmark, STUK, OKG, Ringhals, Chalmers and VTT are following the progress of the work in the project meetings and seminar/workshop organized by NKS-FEMMA. This enables knowledge retention and transfer to the young generation of researchers at all participating organizations. Developing and maintaining the knowledge of DMW-related issues is vital for the Nordic nuclear power industry. NKS-FEMMA creates a unique opportunity to keep close contacts between researchers and nuclear industry.

NKS-FEMMA project achieves high standard of academic excellence. One journal article from NKS-FEMMA project was published in Corrosion Science. Additionally, oral presentations on the NKS FEMMA 2025 project were delivered in the ICG-EAC meeting, NKS Seminar, Environmental Degradation conference and EPRI Alloy 690/52/152 Primary Water Stress Corrosion Cracking Research Collaboration Meeting.

2. Experimental

The specimens precracked and bolt loaded to 20 MPa √ m were exposed in vessels, where the reactor water flows through the loop at a rate of 0.2 kg/s. The electrochemical potential (ECP) of the plant hydrogenated water chemistry (HWC) is around –300 mV/SHE. The hydrogen charging of the feedwater can be up to 0.5–1.5 ppm to keep the ECP measurements that are taken in recirculation loop and main circulation loop below –230 mV/SHE. The temperature and pressure in the test loop were the same as in the reactor pressure vessel, i.e. 275 °C and 7 MPa. The specimens were exposed to hot hydrogenated water during 2001 to 2013 with a total of 81702 h. The reactor was completely shut down in 2013. The test loop and water circulation system were exposed to shutdown water chemistry during 2013–2016. After the shutdown, the hydrogen addition was stopped. There is no circulation during the cold period since the valves were closed. The temperature at the autoclave is suspected to be around 30–40 °C in the post-shutdown periods. The specimens were opened after the exposure first by fatigue and then overloading. The optical microscopy images in Figure 1 reveals a black-color pre-fatigue area and a brown-color crack extension area. With a faster oxide film growth rate at high temperatures due to faster kinetics, the pre-fatigue region exhibits a thicker and thus darker oxide under optical microscopy. The darker pre-fatigue region was supposed to go through the reactor operation periods and also the cold shutdown period while the lighter crack extension region merely occurred during the final cold period.

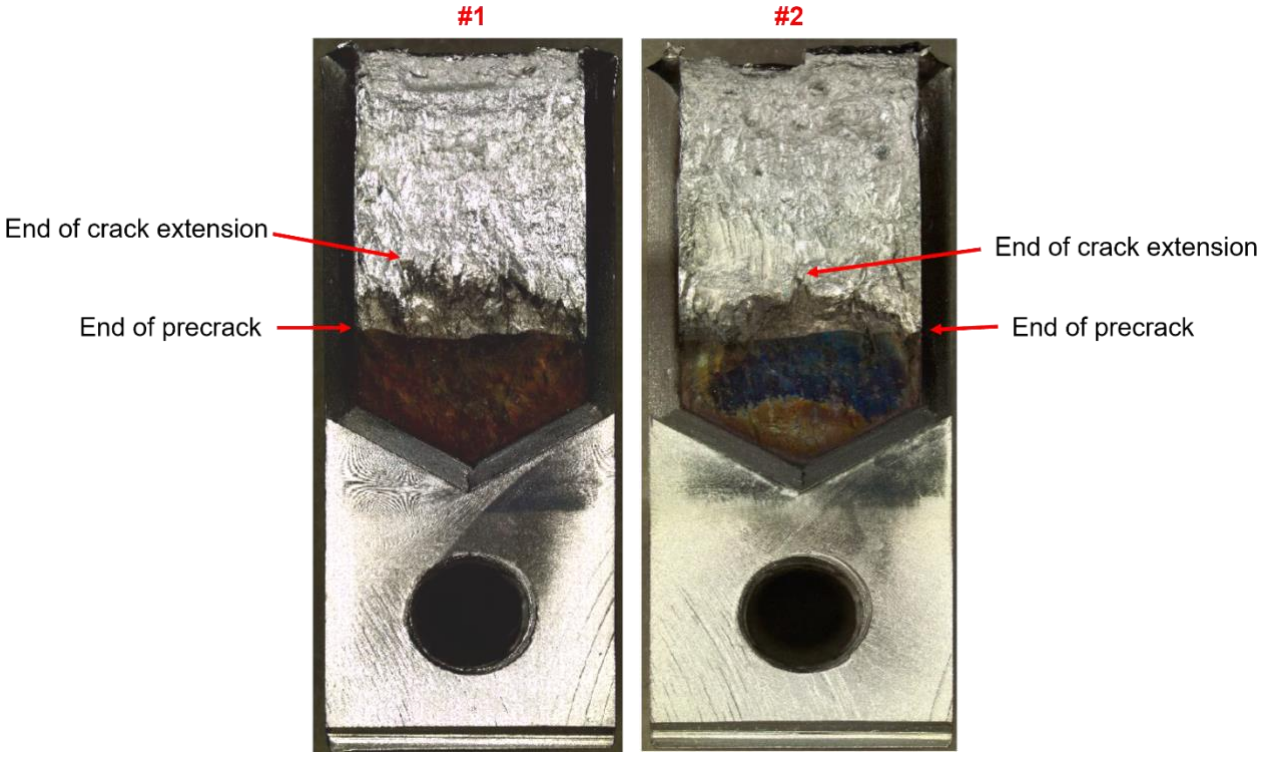

Figure 1: The optical microscopy images of specimens.

3. Fractography investigations

The SEM images of fractography are shown in Figure 2. The pre-fatigue region reveals a much whiter contrast under the backscattered electron detector, which is due to the thicker oxide layers formed on pre-fatigue region during the high-temperature reactor operation periods. It reveals that the cracked region exhibits a similar contrast in brightness as the post-

exposure region with ductile tearing under the backscattered electron detector, which demonstrated that the crack extension region merely occurred during the cold shutdown period. SEM observations of the fracture surfaces of cracked region showed a transgranular fracture mode.

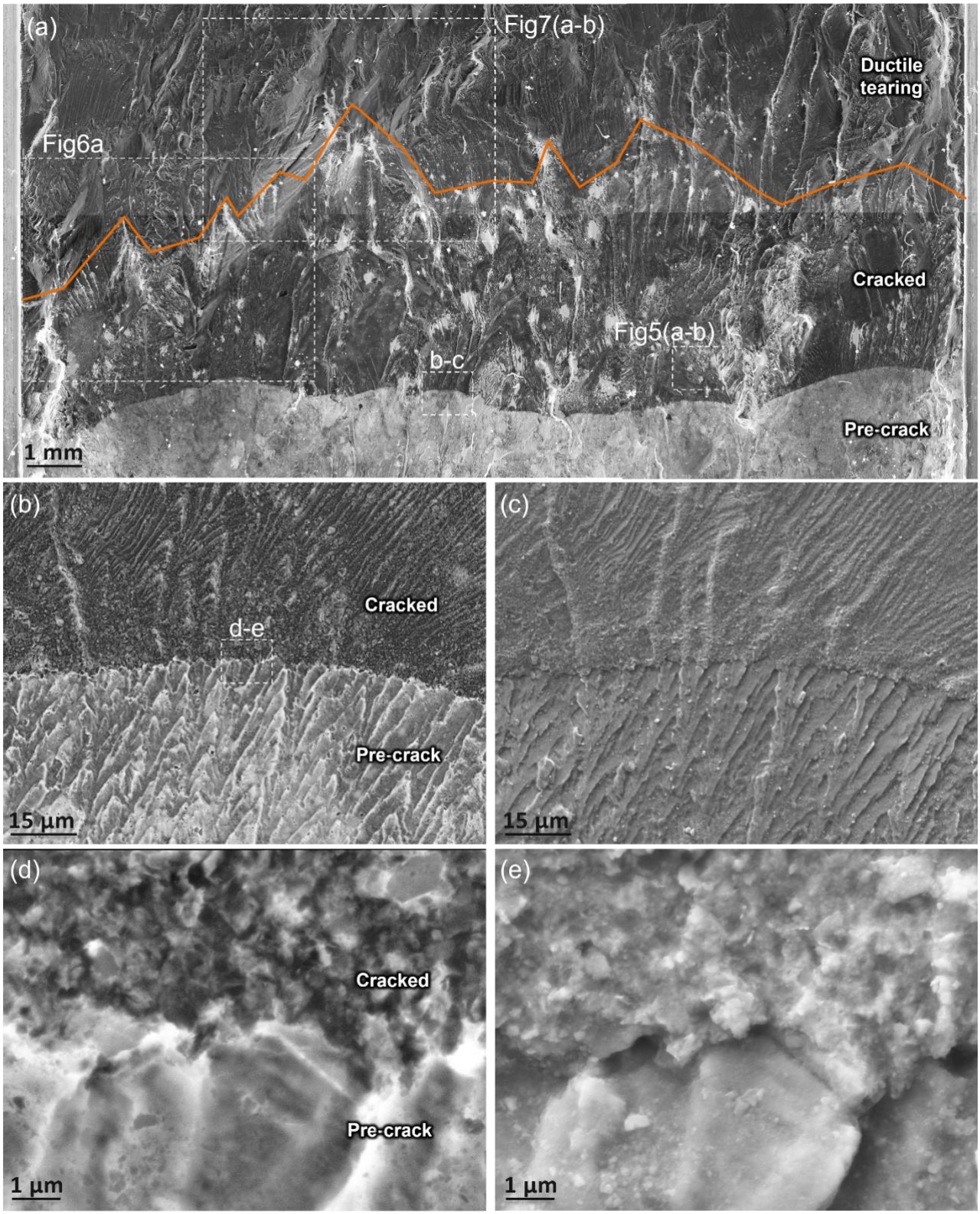

Figure 2: The SEM images of fractography on specimen #1 and the transition line between fatigue pre-crack to cracked region. (a, b and d) images by backscattered electron detector; (c, e) images by secondary electron detector.

4. Cross-sectional investigations

The cross-sectional SEM and EBSD images are shown in Figure 3. As shown in Figure 3(d), extensive secondary cracks were formed in crack-extended region. A very thin oxide layer was observed (the thin-region adjacent to the crack with black contrast in Figure 3(e-g)), particularly in the crack-extended regions, which confirms the decreasing ECP during the cold period. Localized deformation with extensive formation of shear bands in cracked extended region were observed, particularly ahead of the crack tips (Figure 3(h-i)).

In general, the plastic deformation is not localized beneath the main cracked surface, as shown by the cross sectional EBSD aligned with (in Figure 3(b-c)) the crack growth direction. It demonstrates that plasticity is only localized ahead of the crack tips, where extensive shear bands and nano-twins were formed.

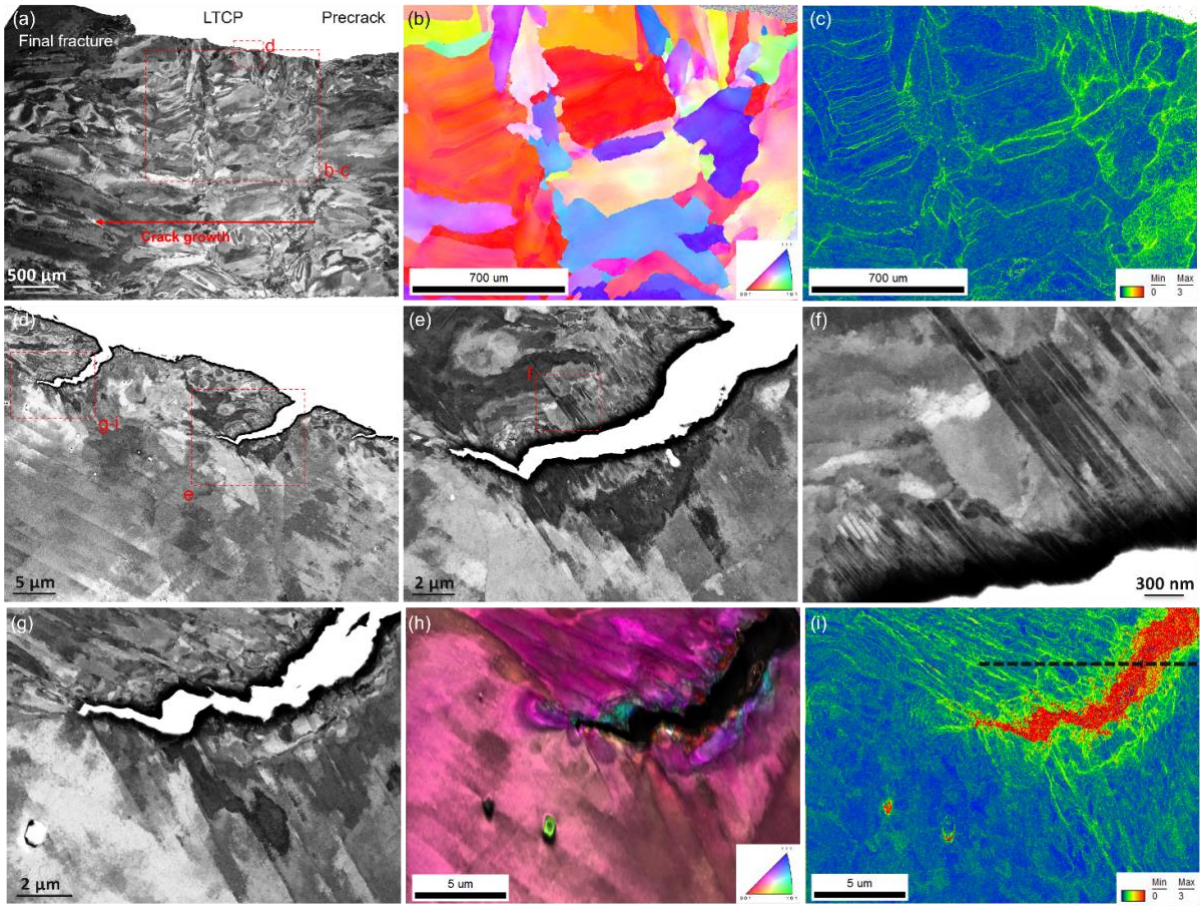

Figure 3: The cross-sectional SEM and EBSD images of specimen #2. The cross sectional was prepared aligned with the crack growth direction. (a, d-g) images by backscattered electron detector; (b, h) IPF figures; (c, i) KAM figures.

5. Discussions

The absence of an intergranular fracture mode in this study can be explained by a limit of hydrogen accumulation at grain boundaries. The transgranular fracture mode indicates that the predominant hydrogen embrittlement in the current system is the hydrogen enhanced localized plasticity (HELP) theory, which describes hydrogen becoming trapped at dislocation

cores. Hydrogen reduces stacking fault energy (SFE), results in localized plasticity and enhances shear bands formation. Hydrogen has been observed to promote stacking fault formation and twinning. Nanoscale microscopy in this study revealed the activation of slip systems at low K levels for Alloy 52 and demonstrated regions of strong localized deformation as the initiation points for the dominant cracks that lead to further failure. This is indicative of local work hardening of the material and a potential increase in the local hydrogen concentration as hydrogen absorbed at the crack surface that accelerates the dislocation movement. As there is no indication of intergranular or interdendritic fracture, this emphasizes that the main interplay of hydrogen-dislocation in the current system is on plasticity localization instead of hydrogen induced grain boundary decohesion.

6. Conclusions

Crack growth of Alloy 52 in HWC cold shutdown water chemistry with relatively fast CGR was observed on constant-displacement bolt-loaded C(T) Alloy 52 specimens at a low K of 20 MPa √ m after exposed in BWR HWC water for 12 years and then in cold shutdown water for a further 3 years in a Swedish NPP unit. The pre-fatigue region was supposed to go through the reactor operation periods and also the cold shutdown period while the crack extension region merely occurred during the final cold shutdown period. The following conclusions can be drawn based on the results obtained.

The unexpected crack propagation in this case under cold shut down period and without external dynamic loading is attributed to LTCP and hydrogen embrittlement. Transgranular fracture was the dominant fracture mode. There was no evident observation of intergranular or interdendritic fracture (negligible HEDE). There were no apparent voids nor carbide-rich fracture surface was observed (negligible HESIV). Hydrogen reduces stacking fault energy, results in localized plasticity and enhances shear bands formation (predominantly HELP).

This work proves that even under very low K levels and low hydrogen concentrations and without dynamic loading, it is possible to reach the threshold for LTCP. The unexpected LTCP phenomena observed in this work is relevant to a real-plant condition and should be considered for evaluating the long-term structural integrity of nuclear components, particularly during extended outage or shutdown scenarios.

7. References

- Pedro A. Ferreirós, Yanling Ge, Björn Forssgren, Mimmi Bäck, Song Lu, Pål Efsing, Zaiqing Que, Unexpected low temperature crack propagation in nuclear shut-down water chemistry of Alloy 52 with potential effects of hydrogen, 2025, Corrosion Science.
- A. Fazi, P. Ferreirós, Y. Ge, S. Lu, M. Thuvander, Z. Que, Unexpected Thermal Aging Effect on Brittle Fracture and Elemental Segregation in Modern Dissimilar Metal Weld, 2024, Materials Characterization 217(1):114419.
- Y. Ge, Z. Que, K. Lindgren, H. Noora, M. Thuvander, Effect of thermal aging on microstructure and carbides of SA508/Alloy 52 dissimilar metal weld, Materials Characterization 200(2023):112880.
- N. Hytönen, Y. Ge, Z. Que, S. Lindqvist, et al., Study of Fusion Boundary Microstructure and Local Mismatch of SA508/Alloy 52 Dissimilar Metal Weld with Buttering, Journal of Nuclear Materials 583(1):154558.

- S. Lindqvist, Z. Que, P. Nevasmaa and N. Hytönen, “The effect of thermal aging on fracture properties of a narrow-gap Alloy 52 dissimilar metal weld,” Engineering Fracture Mechanics, 2023, DOI: 10.1016/j.engfracmech.2023.109056.
- Lindqvist, S., Hytönen, N., Sirkiä, L., Arffman, P., Lydman, J., Ge, Y., Nevasmaa, P. & Que, Z., “Fracture in the Ductile-To-Brittle Transition Region of A Narrow-Gap Alloy 52 and Alloy 52 Dissimilar Metal Weld With Buttering,” ASME PVP, Nov 2022, doi: 10.1115/PVP2022-80690.
- N. Hytönen, Y. Ge, Z. Que, S. Lindqvist, J. Lydman, U. Ehrnstén, P. Rautala, I. Virkkunen and P. Efsing, “Effect of Microstructure on Mechanical Behaviour of Ni-base Alloy Dissimilar Metal Welds,” The 20th International Conference on Environmental Degradation of Materials in Nuclear Power Systems-Water Reactor meeting, ED2021-17104. 2022, Colorado, USA.
- N. Hytönen, Z. Que, S. Lindqvist, J. Lydman, Y. Ge, I. Virkkunen, U. Ehrnstén, P. Rautala, P. Efsing, B. Forssgren, Fusion Boundary Microstructure and Fracture Behaviour of a narrow-gap Alloy 52 Dissimilar Metal Weld and an Alloy 52 Dissimilar Metal Weld with Buttering, International Symposium Contribution of Materials Investigations and Operating Experience to LWRs’ Safety, Performance and Reliability, FONTEVRAUD 10, September 2022, Avignon, France.

Acknowledgements
NKS conveys its gratitude to all organizations and people who by means of financial support or contributions in kind have made the work presented in this report possible.

The authors wish to express their gratitude for the funding and support from Ringhals AB, OKG AB, Teollisuuden Voima Oyj and VTT Technical Research Centre of Finland within the FEMMA+ (Forum for the Effect of Thermal Ageing and Microstructure on Mechanical and EAC Behaviour of Ni-based Alloy Dissimilar Metal Welds Plus) research project. The authors also thank NKS for funding the NKS-FEMMA (AFT/NKS-R(25)134/1) project. The authors would like to thank P. Arffman, J. Lydman, A. Nurmela and L. Sirkiä for the experimental contributions. The authors would like to thank U. Ehrnstén, B. Forssgren, H. Reinvall and H. Hänninen for suggestions and discussions.

Disclaimer
The views expressed in this document remain the responsibility of the author(s) and do not necessarily reflect those of NKS. In particular, neither NKS nor any other organization or body supporting NKS activities can be held responsible for the material presented in this report.

Bibliographic Data Sheet **NKS-511**

Title	Low temperature crack propagation in nuclear shut-down water chemistry of Alloy 52 with potential effects of hydrogen
Author(s)	Zaiqing Que[1], Pedro A. Ferreiros[1], Yanling Ge[1], Sebastian Lindqvist[1], Timo Veijola[1], Mattias Thuvander[2], Björn Forssgren[3] Mimmi Bäck4, Pål Efsing [3, 5]
Affiliation(s)	[1] VTT Technical Research Centre of Finland, 02130 Espoo, Finland [2] Chalmers University of Technology, Department of Physics, SE-412 96, Göteborg, Sweden [3] Ringhals AB, SE-43285 Väröbacka, Sweden [4] OKG AB, 57283 Oskarshamn, Sweden [5] Department of Solid Mechanics, Royal Institute of Technology (KTH), SE-100 44 Stockholm, Sweden
ISBN	978-87-7893-610-3
Date	February 2026
Project	NKS-R FEMMA activity (Contract: AFT/NKS-R(25)134/1)
No. of pages	11
No. of tables	0
No. of illustrations	3
No. of references	8
Abstract max. 2000 characters	Constant-displacement bolt-loaded compact tension specimens of Nickel-based Alloy 52 were exposed to boiling water reactor environment for 12 years and then in cold shutdown water environment for a further 3 years in a Swedish nuclear power plant at a stress intensity factor of 20 MPa √ m. Follow decontamination and specimen opening, unexpected crack extensions of 3 – 4.5 mm were observed. The fracture surface and the cross-sectional deformation microstructure were examined by electron microscopies techniques up to nanoscale. The dominant fracture mode is transgranular along the close-packed {111} planes. Extensive shear bands were observed in vicinity of the crack tips, revealing localized plasticity. Hydrogen reduces stacking fault energy, results in localized plasticity and enhances shear bands formation. Low temperature crack propagation with evident effects of hydrogen was considered as the potential cause of the crack propagation in Alloy 52 without external dynamic loading in cold shut down water chemistry. The project promotes knowledge transfer, improves nuclear materials and fracture mechanics competence and strengthens the connections and experience exchange between the Nordic research organizations, universities, industries, authorities, and especially the young generation. The project deals with structural integrity, long-term operation, and ageing management, which are relevant for both present and future nuclear power plants. The technical results provide a basis for assessment of long-term operation for the Finnish and Swedish

nuclear power plants for both the operators and the regulatory perspectives. Dissemination through the peer reviewed publications and the oral presentations at the international conferences ensured the knowledge exchange in international and Nordic networks.

Key words Dissimilar metal weld, Alloy 52, fusion boundary, characterization, fracture mechanical test, hydrogen embrittlement; low temperature crack propagation

Corrosion Science 261 (2026) 113604

Contents lists available at ScienceDirect

Corrosion Science

journal homepage: www.elsevier.com/locate/corsci

Unexpected low temperature crack propagation in nuclear post-shutdown water chemistry of Alloy 52 with potential effects of hydrogen

Pedro A. Ferreirós [a], Ulla Ehrnstén [a], Yanling Ge [a], Björn Forssgren [b], Mimmi Bäck [c], Song Lu [a], Pål Efsing [b], Zaiqing Que [a,*]

[a] Advanced Materials for Nuclear Energy, VTT Technical Research Centre of Finland, Kivimiehentie 3, Espoo 02150, Finland
[b] Ringhals AB, Väröbacka 43585, Sweden
[c] OKG AB, Oskarshamn 57283, Sweden

ARTICLE INFO

Keywords:
Alloy 52
Hydrogen embrittlement
Low temperature crack propagation
Environmental cracking
Carbonitrides

ABSTRACT

Constant-displacement bolt-loaded compact tension specimens of Nickel-based Alloy 52 were exposed to boiling water reactor environment for 12 years, followed by an additional 3 years in post-shutdown cold water conditions in a Swedish nuclear power plant test loop, under a stress intensity factor of 20 MPa$\sqrt{m}$. After outer surface decontamination and specimen opening, unexpected crack extensions of 3–4.5 mm were observed. The fracture surface and the cross-sectional deformation microstructure were examined by electron microscopies techniques down to the nanoscale. The oxide layer in the region exhibiting unexpected crack growth was notably thin, suggesting that it formed after exposure to elevated operating temperatures. The dominant fracture mode is transgranular, propagating along close-packed {111} planes. The grains contained heterogeneous microstructures with regions enriched in nanometer-sized Ti(N,C) and the zigzag crack paths did not traverse these regions strengthened areas. Extensive shear bands were present near the crack tips, indicating pronounced localized plasticity. Hydrogen reduces stacking fault energy, results in localized plasticity and enhances shear bands formation. Low temperature crack propagation with evident effects of hydrogen was considered as the potential cause of crack propagation in Alloy 52 in the absence of external dynamic loading under post-shutdown cold water chemistry.

1. Introduction

Nickel-Chromium based alloys offer a good combination of corrosion resistance and ductility, with a thermal expansion coefficient in-line with the structural materials being welded. Nickel-based filler metals are routinely employed as weld materials in power generation systems to join bainitic/ferritic low alloy steel (LAS) reactor pressure vessel with austenitic stainless steel pipes [1–5]. It can become a concern for the structural integrity in nuclear power systems, structures and components since several of failures have been observed in such welds in nuclear power plants (NPPs) [6–8]. Moreover, Nickel-Chromium based welds have been suggested to be susceptible to a sub-critical brittle crack propagation in a low temperature aqueous environment termed low temperature crack propagation (LTCP) [9]. This problem can be of high relevance when a reactor goes through a shutdown phase or an extended outage.

The Nickel-based weld metals Alloys 182, 82, 152 and 52 are susceptible to LTCP where typically a reduction of between 50 % and an order of magnitude in fracture toughness compared to in air is observed in pressurized water reactor (PWR) primary water environments with high hydrogen concentrations (~100 mL H_2 / kg H_20 and above). LTCP is widely considered as a hydrogen-induced embrittlement phenomenon that has been observed in laboratory conditions for various Nickel-based alloys at the temperature range of ~50–150 °C in hydrogenated water [10–16].

Among the Nickel-based weld metals, Alloy 182 is normally the most susceptible to LTCP, Alloy 82 slightly less susceptible, and Alloys 52 and 152 seem to be the least susceptible [17]. The effect typically diminishes with decreasing hydrogen concentrations in PWR water and the fracture toughness recovers significantly at a concentration of ~30 mL H_2 / kg H_20 or close to a shutdown hydrogen concentration of ~5–10 mL H_2 / kg H_20 [18]. Ahonen also suggested that Alloy 52 maintains its high fracture resistance with 30 mL H_2/kg H_2O, whereas some specimens of Alloy 52 show a substantial reduction of fracture resistance with a higher

* Corresponding author.
E-mail address: zaiqing.que@vtt.fi (Z. Que).

https://doi.org/10.1016/j.corsci.2026.113604
Received 3 October 2025; Received in revised form 5 December 2025; Accepted 5 January 2026
Available online 6 January 2026
0010-938X/© 2026 The Author(s). Published by Elsevier Ltd. This is an open access article under the CC BY license (http://creativecommons.org/licenses/by/4.0/).

hydrogen content, *e.g.* 100 mL H_2/kg H_2O [16,17]. The typical hydrogen concentrations in plant environments are 5–17 mL H_2 / kg H_20 for boiling water reactor (BWR) hydrogenated water chemistry (HWC), 25–45 mL H_2 / kg H_20 for PWR and 5–10 mL H_2 / kg H_20 during shutdown, respectively. To date, no LTCP incidents involving these Ni-based weld metals have been reported in nuclear power plants in the open literature [16,17]. Nevertheless, low toughness resulting from cooling down to low temperature cannot be completely ruled out, since the absorbed and trapped hydrogen at high temperatures cannot desorb sufficiently to come to equilibrium with a limited environmental hydrogen concentration [18]. However, the knowledge on occurrence and influence of LTCP on fracture and cracking behavior in the Nickel-based filler metals upon long-term plant operation and aging is lacking.

Constant-displacement bolt-loaded compact tension specimens of Nickel-based Alloy 52 were exposed to a BWR HWC environment for 12 years, followed by an additional 3 years in post-shutdown cold water environment in a Swedish nuclear power plant test loop, under a stress intensity factor of 20 MPa$\sqrt{m}$. After outer surface decontamination and specimen opening, unexpected crack extensions of 3–4.5 mm were observed on the specimens. The fracture surface and cross-sectional deformation microstructure were analyzed down to the nanoscale using analytical electron microscopy to elucidate the underlying cracking mechanisms. The intrinsic interactions between microstructure and hydrogen, as well as the resulting localized deformation, were discussed. The implications, relevance and necessary precautions associated with LTCP during reactor shutdown or extended outage conditions were addressed.

2. Experimental procedures

2.1. Materials and specimen

The chemical composition of the materials is provided in Table 1. Two Alloy 52 heats were tested. However, their chemical composition is very similar. Chemical composition analysis was performed using an ARL8860 Optical emission spectrometry (OES) device. Nitrogen and Oxygen were determined according to the carrier gas method "T001–023" using a LECO TC-500 analyzer. The detection limits for C and N contents are 0.05 % and 0.0009 %, respectively. The specimens were pre-cracked in air after machining and subsequently bolt-loaded to an initial stress intensity factor of 20 MPa$\sqrt{m}$. No other loading has been applied to the specimens. The technical drawings and the detailed dimensions of the bolt-loaded compact tension specimens are shown in Fig. 1. The welding direction is into (or out of) the image in Fig. 1 with the crack growing from left to right in the specimen. The crack grew from the weld root area perpendicular to the welding direction.

2.2. Testing procedure

The test loop consists of five pipe shaped vessels (shown in Fig. 2) and reactor water flows through the loop at a rate of 1.0 kg/s or approximately 0.2 kg/s through each vessel. The environment in the test loop is expected to be similar to the reactor water cleanup system (RWCU) system. The purpose of the RWCU is to maintain a high reactor water quality by removing fission products and corrosion products. The electrochemical potential (ECP) of the BWR HWC is around –300 mV/SHE. In the OKG BWR units, hydrogen is injected into the feedwater at levels typically ranging from 0.5 to 1.5 ppm (5.56–16.68 mL H_2/kg

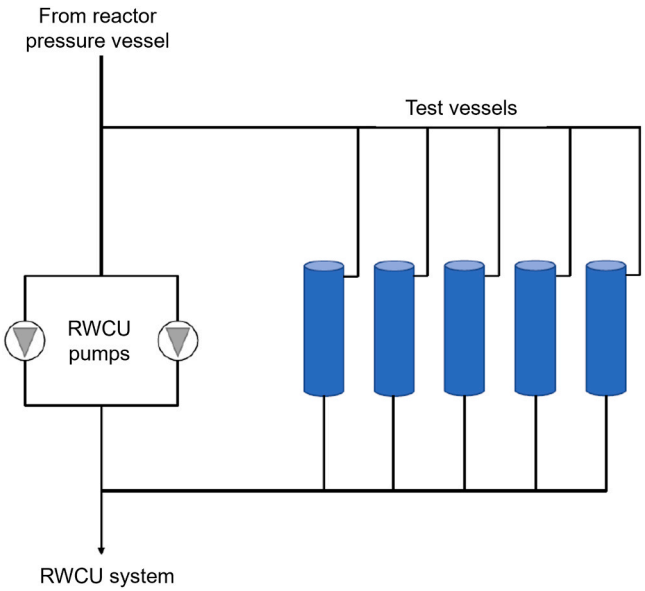

Fig. 1. Technical drawings of the bolt-loaded compact tension specimens (all units in mm).

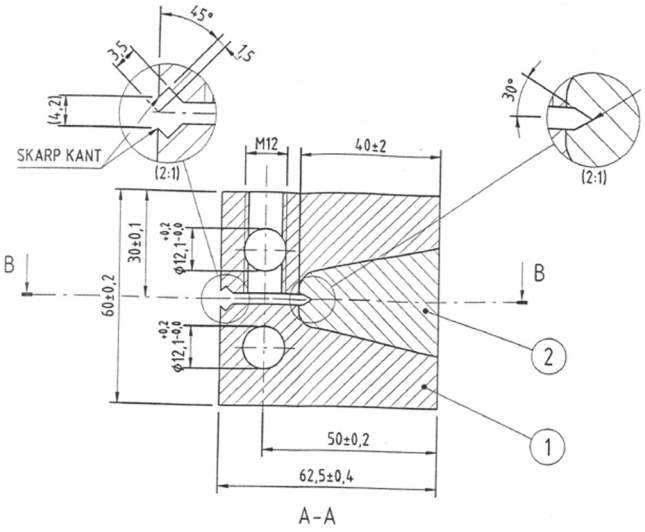

Fig. 2. Illustration plot of the test loop and water circulation system.

H_2O) in order to maintain the electrochemical corrosion potential (ECP), measured in both the recirculation and main circulation loops, below –230 mV/SHE [19]. The temperature and pressure in the test loop were the same as in the reactor pressure vessel, *i.e.* 275 °C and 7 MPa. Table 2 lists the reactor operation periods and the total hot exposure time of the specimens. Therefore, the specimens were exposed to hot hydrogenated water with a total of 81702 h during 2001–2013 (intermittent with down-times of the power plant). No on-line monitoring of crack growth or intermediate inspection of the specimens was possible during the exposure period in the vessels connected to the reactor unit.

The reactor was completely shut down in 2013. The test loop and

Table 1
Chemical composition of the Alloy 52 (wt%).

	Specimen	Heat	C	Cr	Mo	Ni	Mn	Si	P	S	Al	Ti	Cu	Fe	O	N
Alloy 52	#1	NX1681JK	0.020	28.68	0.01	Bal.	0.24	0.12	0.005	<0.001	0.69	0.52	0.01	10.4	0.001	0.012
	#2	NX1573JK	0.024	28.92	0.02	Bal.	0.25	0.15	0.005	<0.001	0.67	0.53	0.01	10.05	0.001	0.01

Table 2
List of reactor operation periods and the exposure time of the specimens.

Period of reactor operation	Operational time (h)	Total hot exposure time (h)
2001–2002	6816	6816
2002–2004	6408	13224
2004–2005	7368	20592
2005–2006	7440	28032
2006–2008	13493	41525
2008	6933	48458
2009	7166	55624
2010	8287	63911
2011	1512	65423
2011–2012	6847	72270
2012–2013	7032	79302
2013	2400	81702

water circulation system were exposed to shutdown water chemistry during 2013–2016. After the shutdown in 2013, hydrogen addition was stopped. There was no circulation in the vessels during the post-shutdown cold period, as the valves connecting the test vessels to the reactor system were closed. ECP, hydrogen content and temperature in the test vessels during the shutdown period were not recorded during this period. The temperature in the test vessels is estimated to be approximately 30–40 °C in the post-shutdown periods. A decreasing ECP is expected during the post-shutdown cold period due to oxygen consumption and hydrogen generation from oxidation reactions.

After removal from the test system, the specimens were glass-blasted for decontamination purposes on the exterior surfaces only. The crack areas were not cleaned to preserve chemical information of the formed oxides. The specimens were subsequently opened after exposure, first by fatigue and then by overloading, and all handling was performed in the hot lab.

2.3. Characterizations

The specimens were analyzed with scanning electron microscope (SEM) and electron backscatter diffraction (EBSD) via a Zeiss Crossbeam 540 SEM with an EDAX HikariPlus EBSD detector. Cross-sectional samples were polished to a 0.05 μm oxide suspension finish. EBSD inverse pole figure (IPF) maps were overlaid with indexing quality maps, and kernel average misorientation (KAM) images (0–3° scale) were analyzed using OIM Analysis 8.6 software. EBSD was conducted with a 200 nm step size, at 20 keV accelerating voltage, 11–13 mm working distance, 70° tilt and 3.0 nA probe current.

To assess the microstructure, cracks and second phases, lamellae were prepared using focused ion beam (FIB) with the Zeiss Crossbeam 540 SEM. After extracting the liftout, the crack gap is filled with Pt to preserve the crack edges during the lamella thinning. The lamellae were investigated using a Thermo Fisher Talos F200X analytical transmission electron microscope (TEM), equipped with the Super-X Energy-dispersive X-ray spectroscopy (EDS) system, operating at 200 kV. High-angle annular dark-field (HAADF) and bright field (BF) images were obtained by Scanning TEM (STEM). Thickness absorption correction was applied to the reported chemical composition of particles acquired by STEM-EDS. The correction used the lamella thickness obtained by converged beam electron diffraction (CBED) method [20]. Representative EDS spectra and detection limits, along with details of the quantification procedure, are included in the supplementary information. Additionally, CBED micrographs to observe the Kikuchi patterns from multiple locations of the lamella were obtained using a camera length of 98 mm. The Kikuchi patterns were compared with simulated patterns using ReciPro v4.903 [21]. The approximate angles (α and β) corresponding to a double-tilt TEM holder were obtained for each Kikuchi pattern to reach the zone axis (ZA) B= [112].

3. Results

3.1. Characterizations and crack growth rate measurement by optical microscopy

The optical microscopy images in Fig. 3 reveal a black-color pre-fatigue area and a brown-color crack extension area. The metallic, shiny region observed under optical microscopy indicates areas that experienced post-test opening in air. With a faster oxide film growth rate at high temperatures due to faster kinetics, the pre-fatigue region exhibits a thicker and thus darker oxide under optical microscopy. The darker pre-fatigue region was supposed to go through the reactor operation periods and the post-shutdown cold period while the lighter crack extension region is assumed to primarily occur during the post-shutdown cold period. Table 3 lists the reactor operation periods and the total exposure time of the specimens. Crack growth rates (CGRs) were calculated under two assumptions: that all crack advance occurred during the high-temperature exposure, or that all of it occurred during the post-shutdown exposure.

3.2. Fractography investigations

SEM images of the fracture surfaces of specimen #1 are shown in Fig. 4 to Fig. 7. In Fig. 4(b,d), the pre-fatigue region displays a noticeably brighter contrast under the backscattered electron detector, consistent with the formation of thicker oxide layers during high-temperature reactor operation. Fig. 4(a) reveals that the crack extended region exhibits a contrast similar to the post-test opening region in air, implying that crack extension occurred primarily during the post-shutdown cold period. The appearance of the fracture surface suggests that crack extension occurred in a single event, with no signs of stepwise macroscopic propagation.

Detailed SEM observations of the crack extended region reveal a predominantly transgranular fracture mode. The fracture surface is characterized by parallel lines typical of intermittent crack growth, extending over large areas across multiple grains. These features are uniform across grains of different orientations and are not consistent with fatigue (*e.g.*, beach marks or fatigue striations) nor with classical transgranular stress corrosion cracking (*e.g.*, cleavage-like facets or river patterns). These observations indicate that the fracture behavior in the crack extended region reflects a distinct deformation and crack propagation mechanism, associated with post-shutdown cold conditions rather than fatigue or conventional SCC.

Fig. 5 shows the detailed fractography on the crack extended region with a 1 mm crack extension. Weld dendritic features can be seen in some local areas but no interdendritic fracture was revealed (Fig. 5(b)).

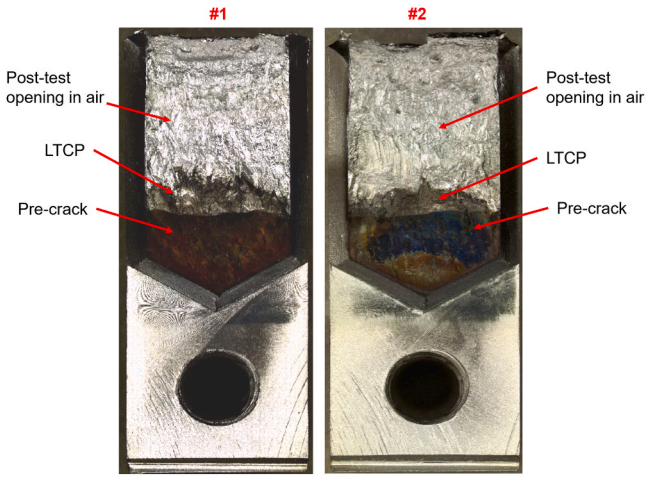

Fig. 3. Optical microscopy images of specimens.

Table 3
List of reactor operation periods and the total exposure time of the specimens.

Specimen	K_{start} (MPa$\sqrt{m}$)	High temperature exposure time (h)	Post-shutdown cold exposure time (h)	Average crack growth length (mm)	CGR assuming all propagation occurred during hot exposure (mm/s)	CGR assuming all propagation occurred during post-shutdown cold exposure (mm/s)
#1	20	81702	26280	4.51	1.53E-8	4.76E-8
#2				3.05	1.04E-8	3.23E-8

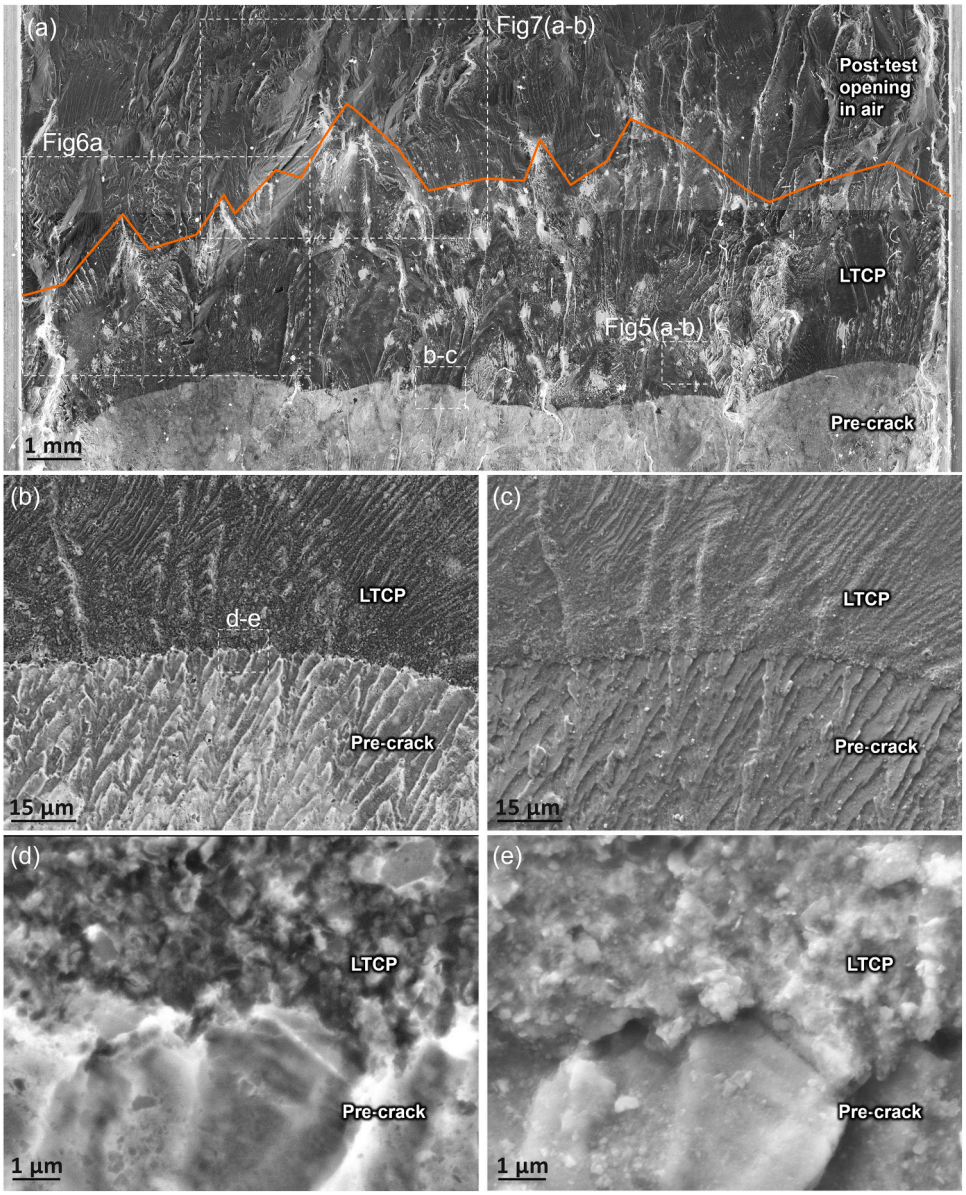

Fig. 4. SEM images of fractography on specimen #1 and the transition line between fatigue pre-crack to cracked region. (a, b and d) images by backscattered electron detector; (c, e) images by secondary electron detector. "Pre-crack", "LTCP" and "Post-test opening in air" indicate regions of pre-cracking, crack extension in post-shutdown cold water, and post-test fatigue and tearing in air, respectively.

Ductile fracture mode with dimples was not observed on the fracture surface.

Fig. 6 presents detailed fractography of the crack extended region with a 3 mm crack extension. Most areas of the crack are very clean, without continuous oxide layers (Fig. 6(a)). SEM observations confirm a transgranular fracture mode, without intergranular or interdendritic features. Some secondary cracks are locally observed (Fig. 6(c-d)).

Fig. 7 depicts the fractography of crack extended regions that are close to the end of the post-shutdown cold exposure period. The precipitates can be observed locally. Fig. 7 reveals that the crack extended region exhibits a similar fracture mode as the post-test opening region in air. In Fig. 7(e-f), precipitate-rich fracture surface was observed locally.

The SEM images of fractography on specimen #2 are shown in Fig. 8. The fracture surface of specimen #2 is generally similar to that of specimen #1. The dominant fracture mode throughout the cracked region is transgranular without ductile dimples. There is no obvious intergranular nor interdendritical fracture. Locally some weld bead

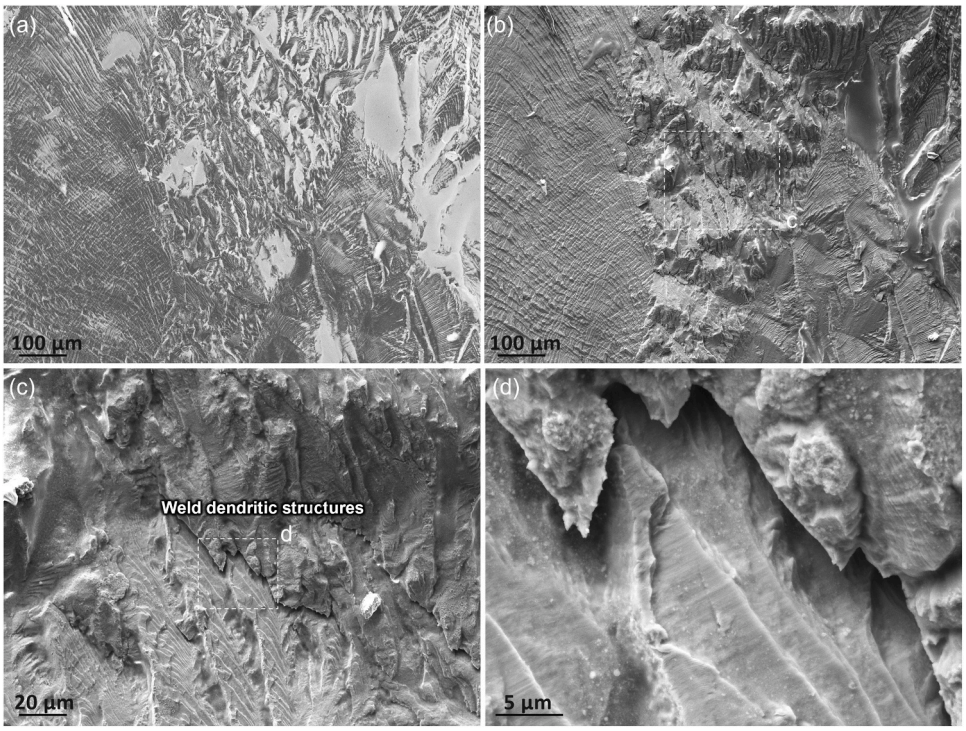

Fig. 5. SEM images of fractography on specimen #1 and the detailed feature on cracked region with a 1 mm crack extension. (a) image by backscattered electron detector; (b-d) images by secondary electron detector.

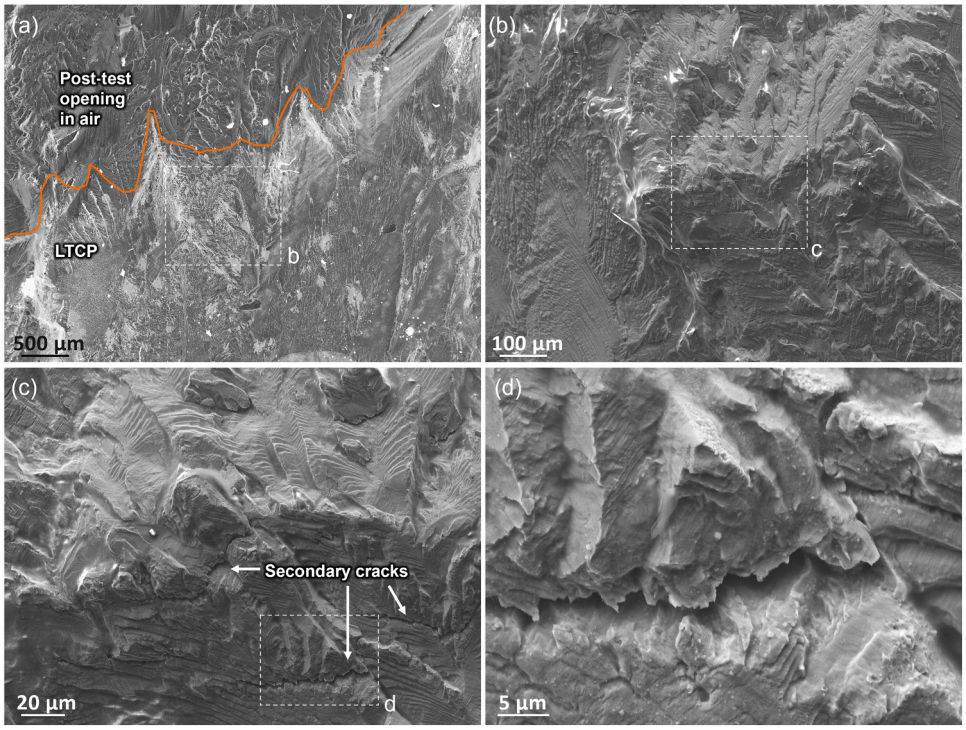

Fig. 6. SEM images of fractography on specimen #1 and the detailed feature on crack extended region with a 3 mm crack extension. (a) image by backscattered electron detector; (b-c) images by secondary electron detector.

structure (Fig. 8(d,g)) or secondary cracks (Fig. 8(h)) are visible. In summary, the fractographic analysis of specimens #1 and #2 indicates a predominantly transgranular fracture mode, with small localized intergranular or interdendritic features accounting for only approximately 1–2 % of the total fracture surface. Additionally, secondary cracking is observed over roughly 3–5 % of the fracture surface.

3.3. Cross-sectional investigations

Cross-sectional SEM and EBSD images of specimen #2 are shown in

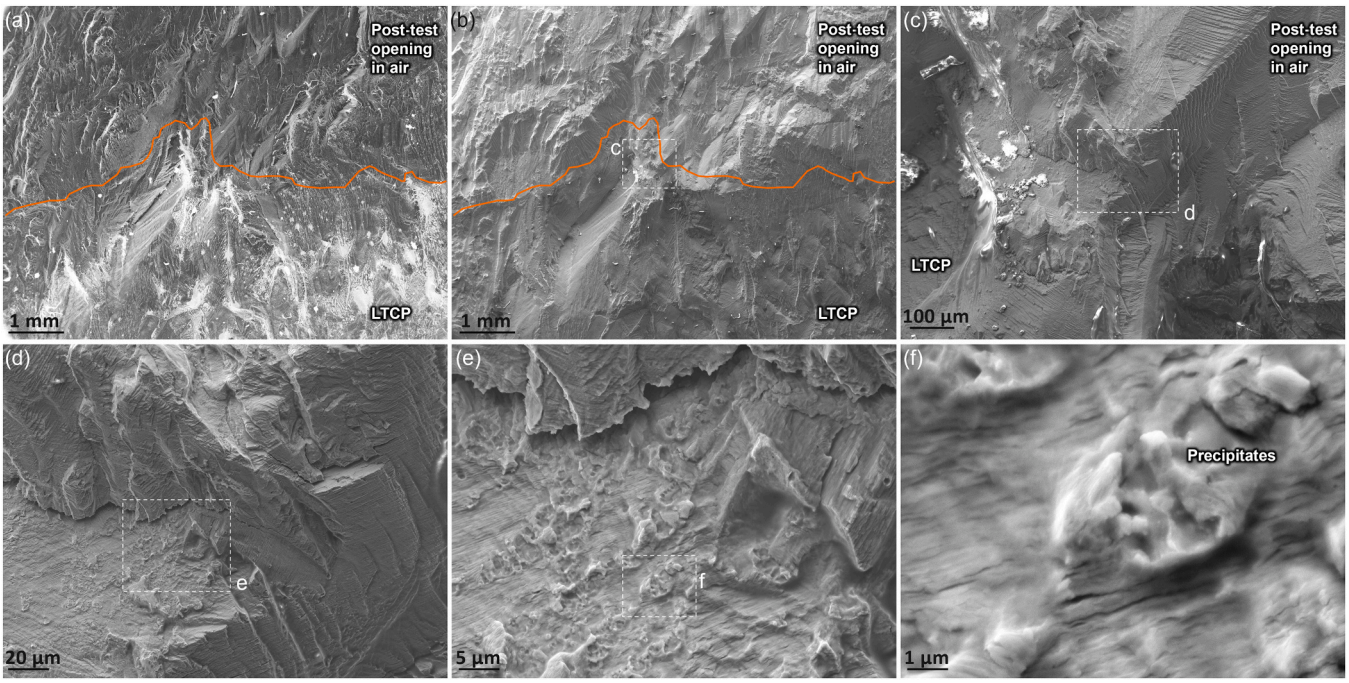

Fig. 7. SEM images of fractography on specimen #1 and the detailed feature on cracked region with a 4 mm crack extension and close to the end of the exposure period. (a) image by backscattered electron detector; (b-f) images by secondary electron detector.

Fig. 9 to Fig. 10. The cross-sections were prepared either parallel or perpendicular to the crack growth direction, as shown in Fig. 9 and Fig. 10, respectively.

As shown in Fig. 9(d), extensive secondary cracks developed in the crack-extended region. A very thin oxide layer is observed in these regions (black contrast in Fig. 9(e-g)), particularly in comparison to the thicker oxide formed in the "pre-crack" region exposed to high-temperature water and the oxide-free "post-test opening in air" region. The observed variations are consistent with a decreasing ECP during the post-shutdown cold period, driven by oxygen consumption and hydrogen generation from oxidation reactions. Oxide thickness is primarily controlled by temperature and time, via kinetic effects, and inversely by ECP, through electrochemical mechanisms.

Localized deformation with extensive formation of shear bands in crack extended region were observed, particularly ahead of the crack tips (Fig. 9(h-i)). In general, the plastic deformation is not localized beneath the main cracked surface, as shown by the cross-sectional EBSD either aligned with (in Fig. 9(b-c)) or perpendicular to (in Fig. 10(b-c)) the crack growth direction. Fig. 10(e-f) demonstrate that plasticity is only localized ahead of the crack tips, where extensive shear bands and nano-twins were formed.

3.4. TEM investigations

A TEM lamella to observe a secondary crack was prepared from specimen #2. The location of the FIB liftout was crossing the crack path, indicated with a dotted line in Fig. 9(i). The STEM on the lamella is showed in Fig. 11. The crack can be clearly observed by the EDS(Pt) map, which shows the Pt deposited on it. There are also some nanometric round SiO particles at the crack, which could be contamination coming from the previous surface polishing process for the EBSD. The EDS maps allow to identify multiple sub-micrometer Fe-oxide particles inside the crack (Fig. 11(c-d)).

A micrometer-size Ti(N,C) is observed in Fig. 11(g-i). The selected area diffraction pattern (SADP) from Fig. 11(f), confirms the face centered cubic (FCC) crystal structure of the Ti-carbonitride with a lattice parameter of a ≈ 4.28 Å. Additionally, the STEM-EDS mapping (Fig. 11(c) and (g)) show a region on the right side of the crack with many dispersed nanometer-size Ti-rich particles. Fig. 11(j-l) show a higher resolution of the EDS maps containing the small particles. The analyses indicate that the nanometer-size particles are also Ti(N,C). The average chemical composition of the two sizes of Ti(N,C) are presented in Table 4. A higher N content and approximately half the C atomic content are observed in the smaller Ti-carbonitrides compared to the micrometer-sized Ti(N,C). The majority of the nanometer-sized Ti(N,C) are cuboidal, measuring about 25 nm, but some are rectangular, measuring 25 nm in one direction and under 100 nm in the other. The Fig. 11(m) shows a SADP from a nanometer-size particle with the matrix oriented near the [100] axis. It is possible to observe a similar orientation of the carbonitride and the matrix (near cube-on-cube orientation relationship) with a higher lattice parameter of the nanometer-size particle respect to the matrix (a ≈ 4.25 Å and a_{Matrix} ≈ 3.60 Å, respectively). The region with nanometer-sized Ti(N,C), probably corresponds to the dendritic weld structure of Alloy 52.

Some authors [22,23] analyzed the particles formed in welds of Alloy 52 using SEM-EDS showing results in agreement with this work. They found similar micrometer-sized Ti(N,C) as the one shown in Fig. 11. Additionally, they reported nanometer-sized precipitates at interdendritic regions and around the micrometer-sized Ti(N,C). The authors refer to these small precipitates as TiN; however, they did not report the chemical composition because their experimental techniques are insufficient to the needed resolution limit.

Fig. 12(a) shows a STEM micrograph of the lamella from specimen #2, with the secondary crack highlighted in color for clarity. Around the crack, the grain in the lamella was oriented along the zone axis (ZA) B= [112]. The FCC matrix exhibits parallel nanometric shear bands in specific directions, with zigzag crystal slip traces corresponding to the close-packed {111} planes. These nanometric shear bands are observed only on the left side of the crack, as shown in more detail in Fig. 13.

Multiple locations of the lamella from Fig. 12(a) were analyzed using CBED to acquire Kikuchi patterns (Fig. 12(b)), from which the tilt angles (α and β angles from the double tilt holder) were determined to reach the ZA. This allowed identification of grain regions that were heavily distorted or rotated due to the crack. Regions with tilt angles above 6° were

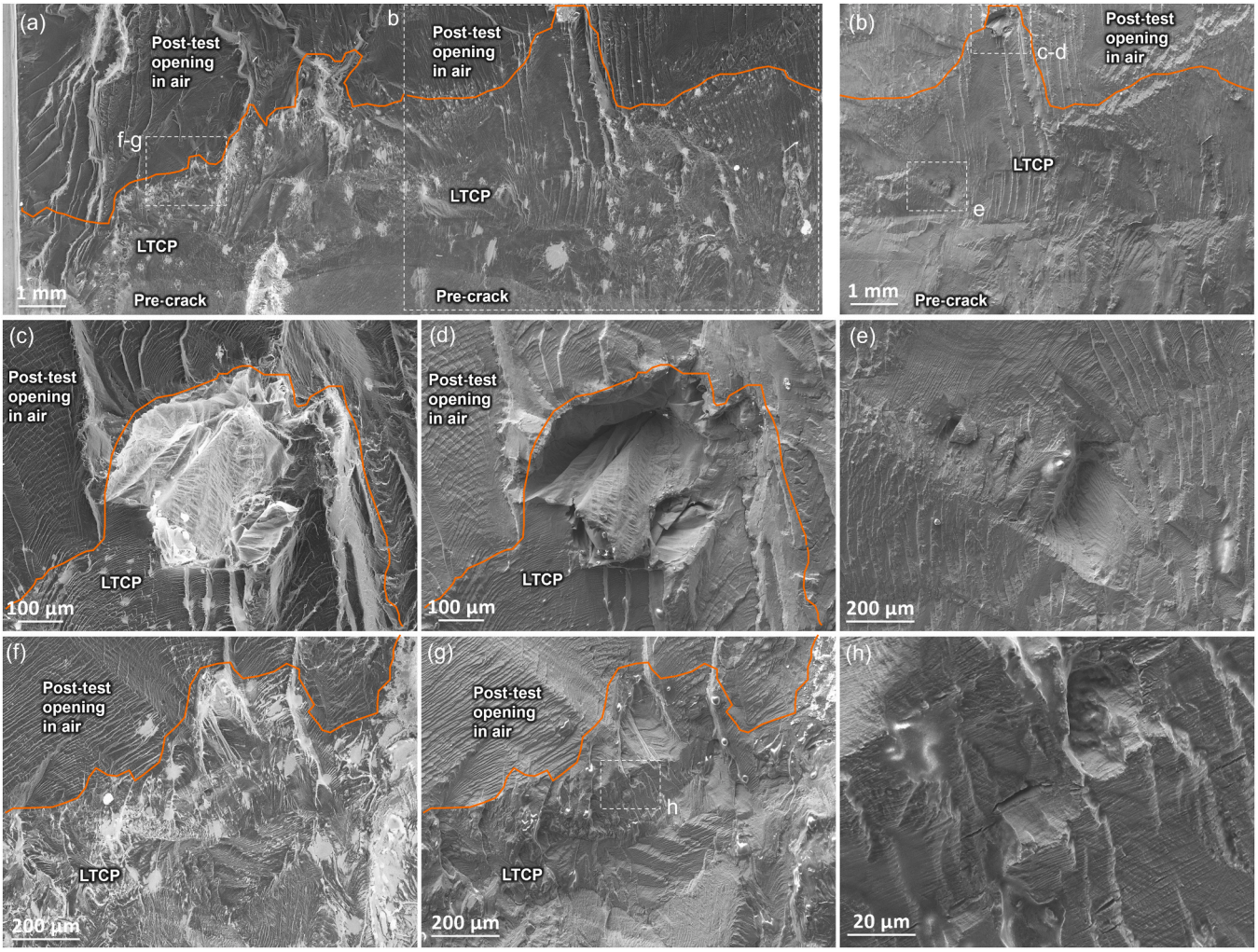

Fig. 8. SEM images of fractography on specimen #2. (a, c and f) images by backscattered electron detector; (b, d-e and g-h) images by secondary electron detector. "Pre-crack", "LTCP" and "Post-test opening in air" indicate regions of pre-cracking, crack extension in post-shutdown cold water, and post-test fatigue and tearing in air, respectively.

considered heavily distorted and were mainly located on the right side of the crack, at a distance of 500 ± 250 nm (see dotted blue line in Fig. 12 (a)). Notably, this heavily distorted region contains no carbonitrides.

EBSD KAM analysis at the lamella location ("dotted line" in Fig. 9(i)) confirms these observations: the left side of the crack shows slip-parallel bands extending over several microns, indicative of higher plastic deformation, whereas only a sub-micron region is heavily deformed on the right side. These results indicate that different deformation processes are acting on the left and right sides of the crack, which can be attributed to the presence or absence of nanometric-sized carbonitrides.

A similar behavior has been reported in other Nickel-based superalloys, where fracture occurs along annealing twin boundaries due to the formation of no-γ″ zone close to the twin boundary and heavy local deformation in this zone [24].

4. Discussion

Optical microscopy revealed a black pre-fatigue region and a brown crack extension region. The darker pre-fatigue area corresponds to thicker oxide layers formed during high-temperature reactor operation, whereas the lighter crack extension region is consistent with growth primarily during the post-shutdown cold period. Backscattered electron imaging confirmed these observations, showing thicker oxides in the pre-fatigue region and much thinner oxide in the crack extension region, indicating that crack growth occurred predominantly at low temperature in a single event. SEM fractography further revealed a transgranular fracture mode with parallel lines extending across multiple grains, without evidence of fatigue striations or transgranular SCC cleavage features. At low temperatures, hydrogen absorption and trapping are enhanced, and the reduced ductility of Ni–Cr alloys limits crack tip blunting, favoring subcritical hydrogen-assisted crack propagation. Collectively, these observations indicate that LTCP is the most probable failure mechanism, while conventional transgranular SCC and fatigue are unlikely.

4.1. Factors influencing LTCP

A number of factors, including hydrogen concentration, loading and K level etc., can influence the LTCP behavior of Nickel-based alloys. This chapter will discuss the factors that can influence LTCP and the correlation/difference to the observations in this work.

Ahonen suggests that Alloy 52 maintains its high fracture resistance in J-R testing with active dynamic loading when exposed to 30 mL H_2/kg H_2O in normal nuclear plant operation, whereas a substantial reduction of fracture resistance can only be observed when exposed to a higher hydrogen content, *e.g.* 100 mL H_2/kg H_2O [16,17]. The LTCP effect was reported to diminish with decreasing hydrogen concentrations and no evident effects can be seen at a concentration of ~30 mL H_2

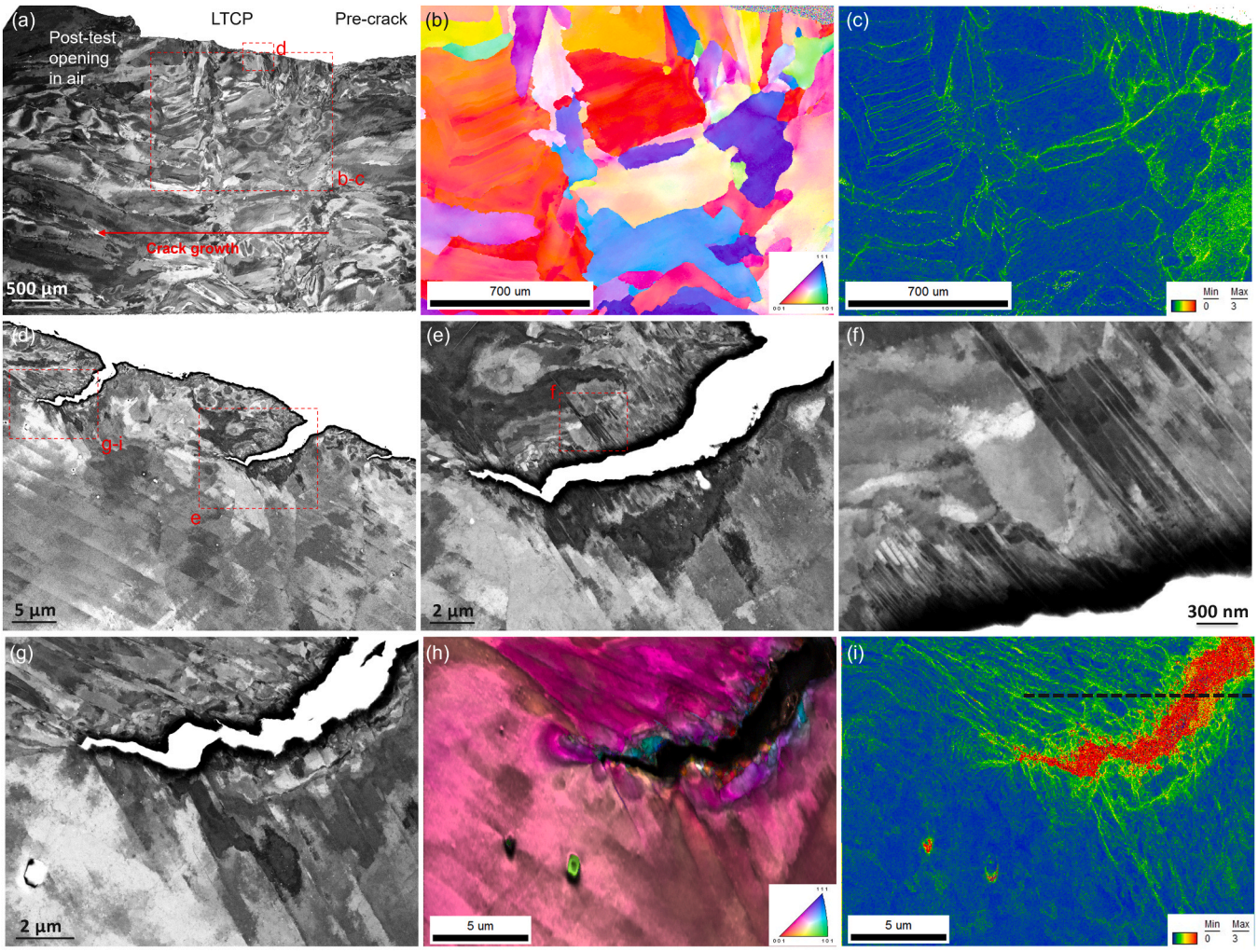

Fig. 9. Cross-sectional SEM and EBSD images of specimen #2. The cross section was prepared aligned with the crack growth direction. (a, d-g) images by back-scattered electron detector; (b, h) IPF figures; (c, i) KAM figures. The dotted line in (i) indicated the location of lamella liftout for TEM.

/ kg H_20 or shutdown water chemistry of ~5–10 mL H_2 / kg H_20 [18]. However, in the current study, the specimens were exposed either to BWR HWC water or shutdown water environment with relatively low hydrogen concentration levels of 0.5–1.5 ppm (5.56–16.68 mL H_2/kg H_2O).

Mills and Brown reported that the lower-bound K_{Pmax} for LTCP of Alloys 52 and 82 are 53 and 40 MPa$\sqrt{m}$, respectively [10,11], where K_{Pmax} represents the maximum stress intensity factor at which LTCP can occur under the given testing conditions. During cooldown tests of constant-displacement bolt-loaded specimens from 288 to 54 °C, LTCP occurred but only at K levels above the material's fracture toughness, K_{JIC} [25]. Under constant-displacement conditions, applied K levels increase by approximately 6 % during cooldown due to an increase in elastic modulus. In the current experiments, the initial stress intensity factor was 20 MPa$\sqrt{m}$, with K decreasing slightly to 16–17 MPa$\sqrt{m}$ by the end of the post-shutdown cold period due to crack propagation. Minor dynamic loading occurred as the plastic zone shifted forward and during thermal transients in the plant operation or the residual stress redistribution during shutdown / cooling, but the K levels remained low compared to those reported in the literature.

Toloczko [26] reported that the CGRs of Alloy 152 at 50 °C in simulated PWR primary water with 29 mL H_2/kg H_2O during cyclic loading were found to be ~2–3 × greater than rates observed at 350 °C at the same stress intensity value of 30 MPa$\sqrt{m}$ and cycling conditions at 0.01 Hz. However, when the test was converted to constant K, the crack in both specimens ceased growing entirely. This suggests that dynamic strain during cycling is required for environment-assisted propagation at this low temperature. However, in this work there was no cyclic loading or external dynamic straining.

With the information given in the above-mentioned literature, the possibility of LTCP effect occurring in the current case should be negligible due to the low hydrogen concentration levels, low K levels and the absence of dynamic straining. However, in this paper, unexpected crack extensions of 3–4.5 mm were observed on constant-displacement bolt-loaded compact tension Alloy 52 specimens at a low stress intensity factor of 20 MPa$\sqrt{m}$ after exposed in BWR HWC environment for 12 years and then in post-shutdown cold water environment for a further 3 years in a Swedish NPP test loop. The underlying fracture mechanism dominated in this case with unexpected crack propagation will be discussed in chapter 4.2.

4.2. *Fracture mode and material-hydrogen interaction for LTCP*

In nuclear environments, three hydrogen-assisted cracking mechanisms can occur. In Hydrogen-Enhanced Localized Plasticity (HELP), hydrogen facilitates dislocation motion, leading to localized slip and accelerated crack propagation [27,28]. In Hydrogen-Enhanced Decohesion (HEDE), hydrogen reduces atomic bond strength, promoting intergranular fracture [29]. In Hydrogen-Enhanced Slip Initiated Voiding (HESIV), hydrogen-enhanced slip induces microvoid nucleation and

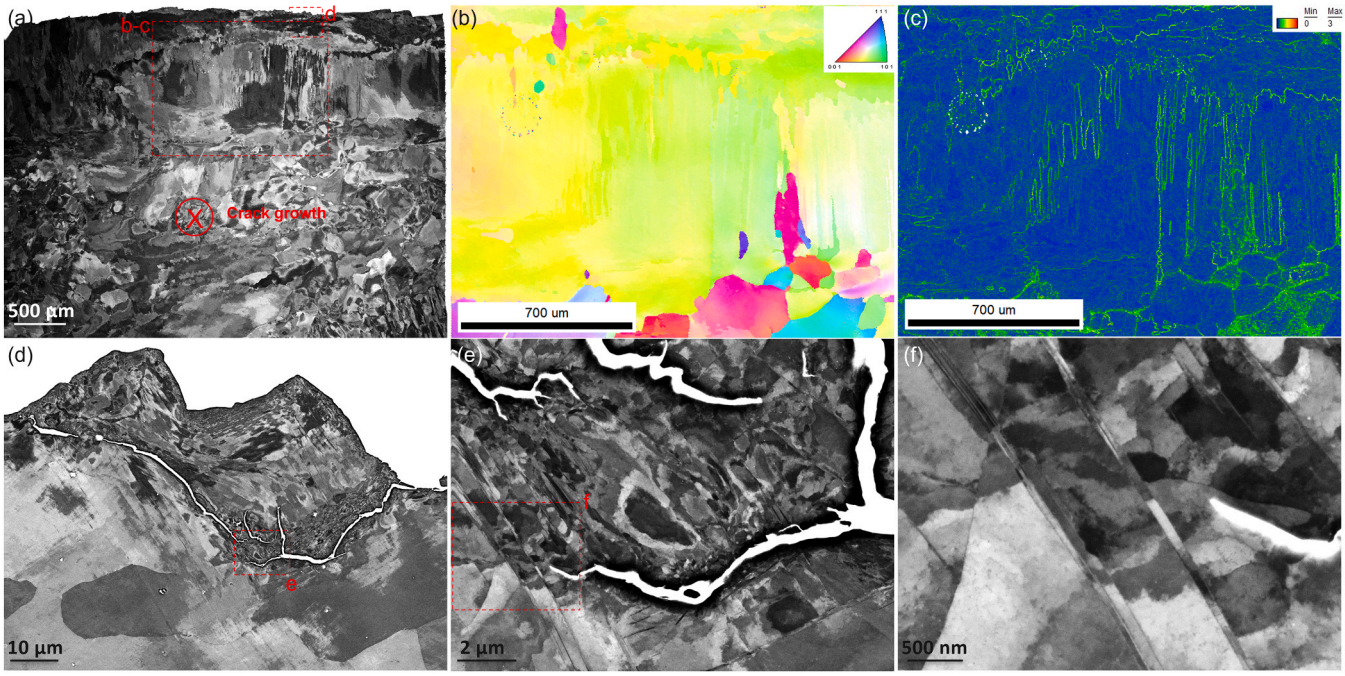

Fig. 10. Cross-sectional SEM and EBSD images of specimen #2. The cross-sectional was prepared perpendicular to the crack growth direction. (a, d-f) images by backscattered electron detector; (b) IPF figure; (c) KAM figure.

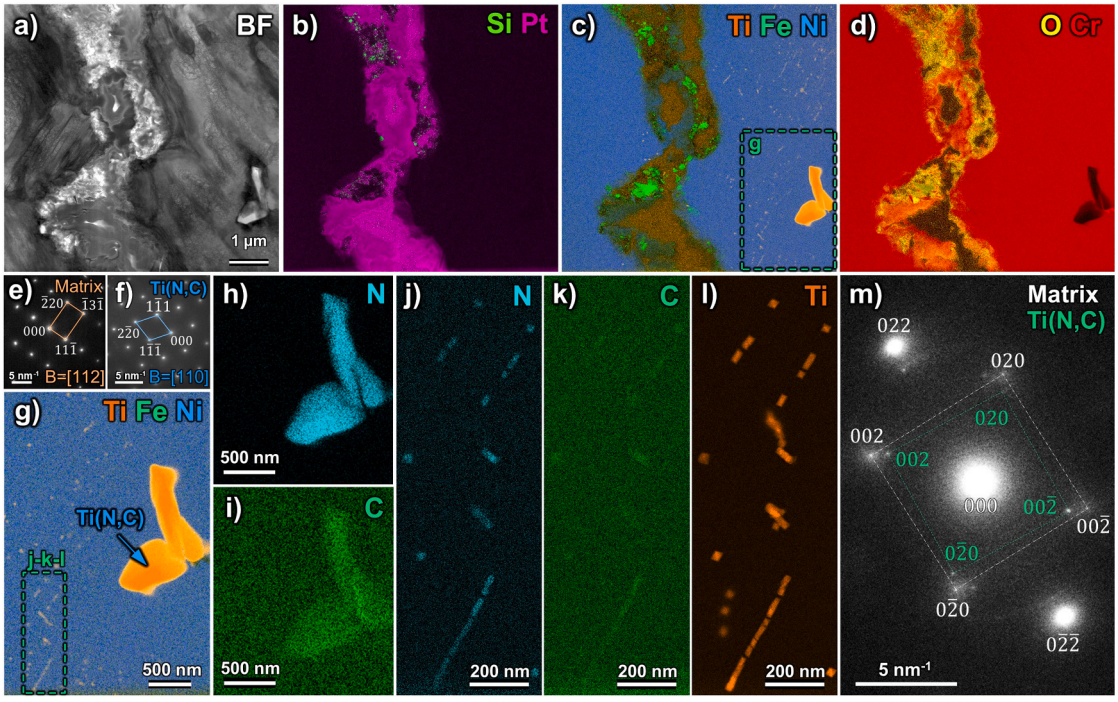

Fig. 11. STEM in a lamella extracted at the crack tip (showed in Fig. 9(g)) from specimen #2. (a) BF STEM and (b-d) STEM-EDS showing the crack. The Pt is deposited on the crack gap during the lamella preparation by FIB. The Si could be coming from the surface polishing process. (e-f) TEM SADPs from the micrometer-sized Ti(N,C) and FCC-matrix, respectively. (g) EDS with both types of Ti(N,C) on the right side of the crack. (h-i) EDS of micrometer-sized Ti(N,C). (j-l) EDS of nanometer-sized Ti(N,C). (m) SADP from a nanometer-sized Ti(N,C) with the matrix oriented near the [100] axis.

coalescence along slip bands, resulting in ductile or quasi-cleavage cracking [18]. The specific mechanism that dominates depends on material, microstructure, stress state, and environment, and their distinction relies on detailed microstructural and fractographic analyses.

STEM provides a deeper understanding of what is happening around the secondary transgranular crack. The grains exhibited a heterogeneous microstructure with regions populated with nanometer-sized Ti(N,C) (see the right side of the crack in Fig. 11). It should be taken into account that the small carbonitrides produce a strengthening of the matrix [30], requiring higher stress to activate the slip systems. Fig. 11 shows carbonitride-free zones on the left side of the crack and in a narrow region (500 nm) to the right side of the crack. These regions also

Table 4
Chemical composition of Ti(C,N) by STEM-EDS. The values were obtained by the average of N# number of precipitates and extracting from there the standard deviation.

Ti(C,N)	N#	Atomic %		
		C	N	Ti
Micrometer-size	3	11.2 ± 1.3	39.0 ± 0.9	49.8 ± 0.8
Nanometer-size	10	22.6 ± 1.8	24.9 ± 6.2	52.5 ± 5.2

exhibited a higher localized plastic deformation by KAM. Assuming that the crack tip is in a precipitate-free region, then a localized plastic field enhanced by hydrogen will produce slip bands in the close-packed planes around the crack. These planes, in turn, are expected to direct transgranular fracture growth. However, when the crack is moving closer to the regions strengthened by carbonitrides crack arrest happens. At this stage, another dense {111} plane is activated, and the crack continues to propagate in regions of the grain that are largely free of precipitates. Consequently, the crack tip advances along {111} planes in a zigzag path (Fig. 12(a)), avoiding the nanoprecipitate-strengthened region (Fig. 11). STEM micrographs indicate that these carbonitride-rich regions act as zones of higher crack resistance within the weld structure. While most literature on LTCP reports an intergranular fracture mode, the transgranular or interdendritic fracture observed here reflects the influence of the microstructure on crack evolution. This difference highlights the role of material–hydrogen interactions and suggests that the fracture mode depends on the local interplay between precipitate distribution, grain structure, and hydrogen-assisted deformation mechanisms.

J_{IC} and tearing moduli were reported to reduce by one to two orders of magnitude for Alloy 52 exposed in water with 150 mL H_2/kg H_2O of H_2 at 54 °C [11]. Such specimens showed negligible or no plasticity prior to cracking, hence the toughness degradation is attributed to a hydrogen-induced intergranular cracking mechanism. A similar degree of embrittlement and cracking mechanism observed in low-temperature water can be reproduced in hydrogen-precharged specimens tested in air [10], which demonstrates that LTCP is a hydrogen-embrittlement mechanism. In the above-mentioned intergranular fracture cases, hydrogen from the water reduces the grain boundary cohesive strength and promotes planar slip, which localizes strain concentration along grain boundaries. Similarly, with a shutdown water chemistry with 10–30 mL H_2/kg H_2O of H_2 at the temperature of 54 °C, the less LTCP-resistance Alloy 82 experienced a significant reduction in toughness and exhibited a mixed-mode fracture (interdendritic and ductile)

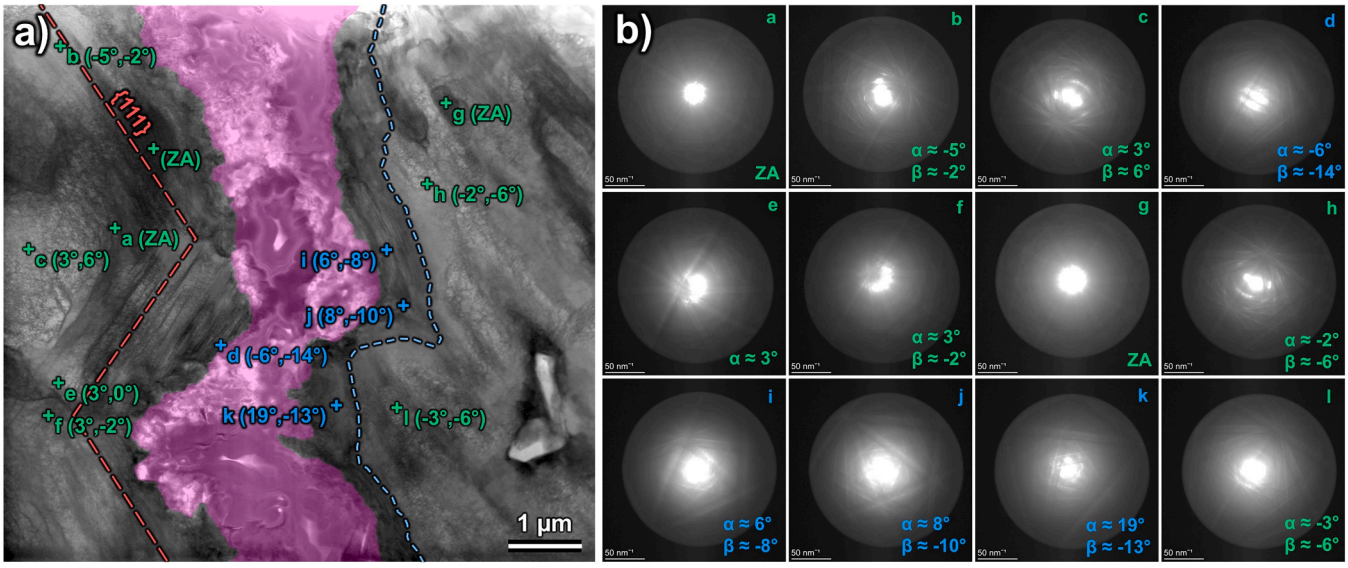

Fig. 12. BF STEM of a crack from specimen #2. (a) The crack was colored for easy identification. Slip planes of {111} forming a zigzag pattern are visible parallel to the crack. The grain in the lamella was oriented around the zone axis (ZA) B= [112]. The tilt angles corresponding to a TEM double tilt holder (α and β) to reach the ZA at multiple sites of the lamella are indicated. (b) CBED micrographs of Kikuchi patterns corresponding to the locations indicated in (a).

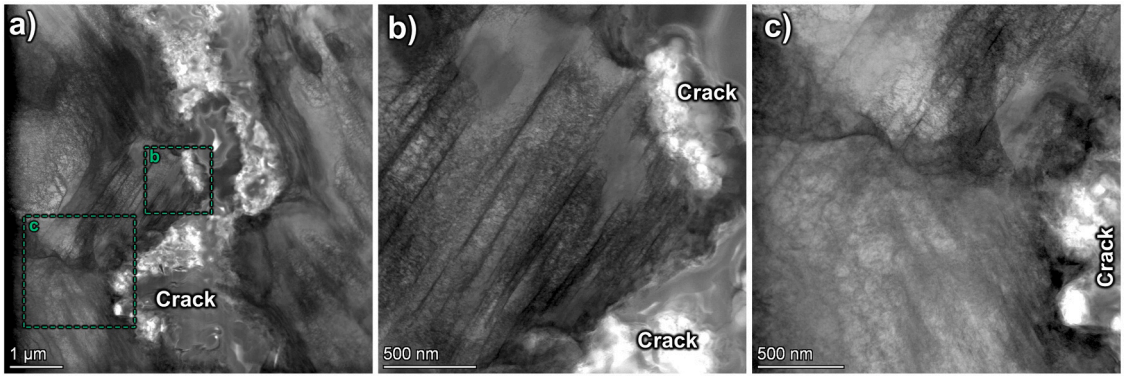

Fig. 13. BF STEM micrographs of a crack from specimen #2. (a) Full view of the crack. (b-c) Higher magnification details showing the parallel slip traces that follow the crack path on its left side (region without Ti-carbonitrides).

under high strain conditions [12]. Overall, these observations showed that hydrogen-induced intergranular decohesion process (*i.e.* HEDE) can occur during LTCP in Nickel-based alloys when a sufficient amount of hydrogen at the grain boundaries was reached [29]. Martin *et al.* demonstrated the crucial role of deformation processes in establishing sufficient concentration of hydrogen at the grain boundaries [31].

The absence of an intergranular fracture mode in this study can be explained by a limit of hydrogen accumulation at grain boundaries. The transgranular fracture mode indicates that the predominant hydrogen embrittlement in the current system is the HELP theory, which describes hydrogen becoming trapped at dislocation cores. Hydrogen reduces stacking fault energy (SFE), results in localized plasticity and enhances shear bands formation. Hydrogen has been observed to promote stacking fault formation, twinning and even martensitic transformation in austenitic alloys [27,28]. For example, stacking faults were observed to expand due to the interaction with H in a high Mn austenitic steel [32] and in a high entropy alloy [27]. Ferreira et al. [33] observed the expansion of dislocation notes at the presence of hydrogen in a 310 austenitic stainless steel. Hydrogen assisted deformation twinning was observed in steels [34,35] and high entropy alloys [36]. Theoretical calculations by interatomic potentials [37] and ab initio [38] also predicted that hydrogen reduces the SFE. Overall, the above experimental and theoretical studies may suggest that in the present Ni based alloys with relatively high SFE (compared to metastable stainless steels [39]) hydrogen may promote deformation localization through the reduction of the SFE or the interaction with partial dislocations [35].

Nanoscale microscopy in this study revealed the activation of slip systems at low K levels for Alloy 52 and demonstrated regions of strong localized deformation as the initiation points for the dominant cracks that lead to further failure. This is indicative of local work hardening of the material and a potential increase in the local hydrogen concentration as hydrogen absorbed at the crack surface that accelerates the dislocation movement. Ebner [40] reported an increase in strain rate sensitivity and decrease of the activation volume as a consequence of hydrogen charging in Nickel-based alloy, which indicates an increase in lattice friction, a promotion of planar slip and a more localized deformation. The enhanced dislocation movement can be further promoted by the strong tri-axial elastic strain field and the numerous dislocation strain fields adjacent to the crack tip [9]. As there is no indication of intergranular or interdendritic fracture, this emphasizes that the main interplay of hydrogen-dislocation in the current system is on plasticity localization instead of hydrogen induced grain boundary decohesion.

Herms [14] showed that the duration of pre-exposure to high-temperature primary water did not significantly influence the fracture toughness of the Nickel-based alloy, which is in agreement with Ahonen *et al.* [17]. This suggests that bulk hydrogen diffusion is not the critical elementary mechanism for LTCP, which mainly depends on the localization of hydrogen ahead of the crack tip [41]. Richey [42] reported that the LTCP rate of Alloy 82 displays a weak, negative temperature dependence with an apparent activation energy of –8.8 kJ/mol between 25 and 150 °C. This temperature dependence is contrary to previous work on Alloy X750 that suggested a relatively strong (+47.3 kJ/mol) temperature dependence for LTCP that correlated with the activation energy for hydrogen diffusion in Nickel. It indicates that the rate of LTCP crack propagation is not generally limited by solid state diffusion of hydrogen. Mechanistically, this suggests that hydrogen embrittlement occurs very near the crack tip surface and relatively fast CGRs can thus be supported, as what was observed in this work.

In addition to hydrogen-promoted dislocation mobility, hydrogen could result in the enhancement of the strain-induced generation of vacancies, *i.e.* the HESIV mechanism. HESIV is normally connected to the precipitates since the vacancies and voids can be generated at the precipitate-matrix interfaces. Carbide interfaces seem to be implicated as preferred traps for hydrogen in Nickel-based alloys and thus the resulting embrittlement can be aggravated [18,43]. The desorption activation energy of lattice hydrogen and hydrogen trapped at dislocations in the matrix, hydrogen trapped at vacancies and the hydrogen trapped at carbide/matrix interface is 33.5 kJ/mol, 47.6 kJ/mol and 65.9 kJ/mol, respectively [44]. Ahonen reported that intergranular carbide-rich fracture surface layer was repeatedly observed in LTCP studies of Alloy 52 [16,17]. However, there are no significant voids nor evident carbide-rich fracture surface observed in this work. Based on the above discussions, the predominant hydrogen embrittlement mechanism is HELP whereas HESIV or HEDE only play a minor role.

4.3. The implication of this study to industry

Contrary to most LTCP-relevant literature where simulated light water reactor environments or hydrogenated specimens by hydrogen pre-charging was used, the BWR HWC environment in the test loop in this work was connected to the RWCU system and thus the practical BWR reactor water flowed through the loop. Furthermore, in all available literature either J-R tests with active dynamic loading, specimens with cyclic loading or constant-displacement bolt-loaded specimens at high K levels were applied. Peng [45] investigated the LTCP behavior of 25 % cold worked Alloy 690 in 50 °C water and the CGR under trapezoidal loading condition ($K_{max} = 35\ MPa\sqrt{m}$, R = 0.7) was reported as $< 2.2{\cdot}10^{-9}$ mm/s, which is much lower than the LTCP CGR reported in this work. Sakima [46] presented a LTCP susceptibility map of Alloy 152 weld metal constructed by result of J-R tests and reported that Alloy 152 weld metal is not susceptible to LTCP in water with dissolved hydrogen content of less than 15 mL H_2/kg H_2O at 50 °C. Therefore, they judged that there is no necessity of countermeasures for LTCP from a viewpoint of maintenance assessment, as there was no plant operation condition in 50 °C water with dissolved hydrogen content of over 15 mL H_2/kg H_2O. It was evaluated that there is very little possibility that LTCP becomes a threat in actual PWRs. The LTCP phenomena observed in this work may be relevant to real-plant conditions and warrant consideration when evaluating the long-term structural integrity of nuclear components, particularly during extended outages or shutdown periods. The study indicates that even at relatively low stress intensity factors and low bulk hydrogen concentrations, and in the absence of external dynamic loading, conditions may exist that approach the apparent K threshold for LTCP.

Ahonen reported that thermally aged Alloy 52 specimens (aged for 10,000 h at 400 °C, equivalent to an operation of 60 years at 288 °C) show more local intergranular areas of LTCP propagation than the non-aged materials [16,17], which indicates a thermal aging effect. Long-term thermal aging at the NPPs can lead to significant elemental segregation to grain boundaries and carbide coarsening [47], which can enhance grain boundary decohesion, facilitate brittle crack propagation and enhance LTCP effect. This shows that for NPPs that are aiming for lifetime extension beyond 60 or 80 years, there is a potential risk of stronger LTCP effects.

As shown in this work, a strong tri-axial elastic strain field, rather than the solid state diffusion of hydrogen, is a key factor for LTCP and HELP of Nickel-based alloys. A sharp pre-crack appears necessary for LTCP to initiate [43]. In operational components, stress corrosion cracking [48] or fatigue cracks [49] could act as prerequisites or promoters for LTCP. Factors influencing intergranular stress corrosion cracking in PWRs and BWRs include the degree of cold working, residual deformation, water impurity content, and residual and applied stress [50]. Although low cycle fatigue is considered in the design codes of NPPs, environmental effects were not explicitly accounted for until recently in the nuclear operation. Low cycle fatigue damage in NPPs primarily arises from non-monotonic cyclic loading associated with thermal transients, load-following, thermal stratification, and occasional plant shutdowns and start-ups [49]. To minimize the risk of LTCP in operational plants, measures to mitigate stress corrosion cracking and fatigue initiation should be considered [50].

5. Conclusions

Crack growth in Alloy 52 under BWR HWC post-shutdown cold water chemistry, with a relatively fast CGR, was observed on constant-displacement bolt-loaded C(T) specimens tested at a low K of 20 MPa$\sqrt{m}$. These specimens had been exposed to BWR HWC water for 12 years, followed by an additional 3 years in post-shutdown cold water in a Swedish NPP test loop. The pre-fatigue region is expected to have developed during reactor operation and the post-shutdown cold period, whereas the observed crack extension region predominantly occurred during the post-shutdown cold period. Based on the results obtained, the following conclusions can be drawn:

- The observed crack propagation during the post-shutdown cold period, in the absence of external dynamic loading, is consistent with LTCP assisted by hydrogen.
- Transgranular fracture was the dominant fracture mode. There was no evident observation of intergranular or interdendritic fracture (negligible HEDE). There were no apparent voids nor carbide-rich fracture surface was observed (negligible HESIV).
- Hydrogen reduces stacking fault energy, results in localized plasticity and enhances shear bands formation (predominantly HELP).
- The grains exhibited heterogeneous microstructures containing regions populated by nanometer-sized Ti(N,C). Crack propagation occurred along zigzag paths on the close-packed {111} planes, without crossing the regions strengthened by carbonitrides.
- LTCP is not limited by solid state diffusion of hydrogen and hydrogen embrittlement occurs in adjacent to the crack tip.
- These findings indicate that even at relatively low stress intensity factors and low bulk hydrogen concentrations, conditions may exist that approach the apparent K threshold for LTCP.
- While based on a limited number of specimens and without direct hydrogen measurements, these observations suggest potential relevance to real-plant conditions and warrant further investigation when evaluating the long-term structural integrity of nuclear components, particularly during extended outages or shutdown periods.

CRediT authorship contribution statement

Pedro A. Ferreirós: Writing – original draft, Methodology, Investigation, Formal analysis, Data curation. **Ulla Ehrnstén:** Writing – review & editing, Methodology, Investigation. **Yanling Ge:** Investigation, Formal analysis, Data curation. **Björn Forssgren:** Writing – review & editing, Investigation. **Mimmi Bäck:** Writing – review & editing, Investigation. **Song Lu:** Writing – review & editing, Investigation. **Pål Efsing:** Writing – review & editing, Investigation. **Zaiqing Que:** Writing – review & editing, Writing – original draft, Resources, Project administration, Methodology, Investigation, Formal analysis, Data curation, Conceptualization.

Declaration of Competing Interest

The authors declare that they have no known competing financial interests or personal relationships that could have appeared to influence the work reported in this paper.

Acknowledgements

The authors wish to express their gratitude for the funding and support from Ringhals AB, OKG AB, Teollisuuden Voima Oyj and VTT Technical Research Centre of Finland within the FEMMA+ (Forum for the Effect of Thermal Aging and Microstructure on Mechanical and EAC Behavior of Ni-based Alloy Dissimilar Metal Welds+) research project. The authors also thank NKS for funding the NKS-FEMMA (AFT/NKS-R (25)134/1) project. The authors would further like to thank T. Lehtikuusi, H. Reinvall and H. Hänninen for suggestions and discussions.

Appendix A. Supporting information

Supplementary data associated with this article can be found in the online version at doi:10.1016/j.corsci.2026.113604.

Data availability

Data will be made available on request.

References

[1] W.-C. Chung, J.-Y. Huang, L.-W. Tsay, C. Chen, Microstructure and stress corrosion cracking behaviour of the weld metal in Alloy 52-A508 dissimilar welds, Mater. Trans. 52 (1) (2011) 12–19.
[2] J. Gao, J. Tan, M. Jiao, X. Wu, L. Tang, Y. Huang, Role of welding residual strain and ductility dip cracking on corrosion fatigue behavior of Alloy 52/52M dissimilar metal weld in borated and lithiated high-temperature water, J. Mater. Sci. Technol. 42 (2020) 163–174.
[3] Y. Ge, Z. Que, K. Lindgren, N. Hytönen, M. Thuvander, Effect of thermal aging on microstructure and carbides of SA508/Alloy 52 dissimilar metal weld, Mater. Charact. 200 (112880) (2023).
[4] Z. Que, S. Lindqvist, N. Hytönen, Y. Ge, P. Nevasmaa, J. Lydman, L. Sirkiä, P. Arffman, A. Forsström ja U. Ehrnstén, Forum for the effect of thermal aging and microstructure on mechanical and EAC behaviour of Ni-base alloy dissimilar metal welds (FEMMA), in: VTT Technology, 420, Espoo, Finland, 2023.
[5] N. Hytönen, Y. Ge, Z. Que, S. Lindqvist, P. Nevasmaa, I. Virkkunen, P. Efsing, Study of Fusion Boundary Microstructure and Local Mismatch of SA508/Alloy 52 Dissimilar Metal Weld, J. Nucl. Mater. 583 (154558) (2023).
[6] P. Efsing, B. Forssgren and R. Kilian, Root cause failure analysis of defected J-groove welds in steam generator drainage nozzles, in Proceedings of the Twelfth International Conference on Environmental Degradation of Materials in Nuclear Power Systems-Water Reactors, 2005.
[7] A. Jenssen, K. Norrgard, J. Lagerstrom, G. Embring, C. Jansson and P. Efsing, Structural assessment of defected nozzle to safe-end welds in Ringhals-3 and -4, in Proc. Fontevraud V Intl. Symp., 2000.
[8] P. Efsing and J. Lagerström, Analysis of a defected dissimilar metal weld in a PWR power plant, in 10th Int Conf Nucl Eng, 2002.
[9] P. Platt, J. Sayers, D. Horner, A. Barrow, D. Engelberg, Hydrogen-induced brittle fracture in nickel based alloy 82 weld metal, Corros. Sci. 153 (2019) 118–126.
[10] W. Mills, C. Brown, Fracture toughness of Alloy 600 and EN82H weld in air and water, Metall. Mater. Trans. A 32A (5) (2001) 1161–1174.
[11] C. Brown, W. Mills, Fracture toughness of Alloy 690 and EN52 welds in air and water, Metall. Mater. Trans. A 33A (6) (2002) 1725–1735.
[12] B. Young, Reduction of Toughness for Weld Metal in a PWR Primary Water Environment with Varying Dissolved Hydrogen, Lithium and Boric Acid Concentrations, in Proceedings of the 12th International Symposium on Environmental Degradation of Materials in Nuclear Power Systems - Water Reactors, Salt Lake City, Utah, USA, 2005.
[13] A. Mclllree, Effects of Hydrogen and Tem-perature on the Fracture Resistance of Weld Metals 182 and 152 in Simulated PWR Shutdown Environment, in Proceedings of the 6th Fontevraud Conference, Fontevraud Royal Abby, France, 2006.
[14] E. Herms, LTCP of Alloy 182/152 Test-ed in PWR Primary Water, in Proceedings of the 14th International Symposium on Environmental Degradation of Materials in Nuclear Power Systems - Water Reactors, Virginia, USA, 2009.
[15] Q. Peng, Environmentally Assisted Crack Growth in One-Dimensionally Cold Worked Alloy 690TT in Primary Water, Corros. Sci. 57 (2012) 81–88.
[16] M. Ahonen, Low Temperature Crack Propagation (LTCP) Susceptibility of Nickel-Based Alloy 182, 152 and 52 Weld Metals in PWR Primary Water, in Proceedings of the 16th International Conference on Environmental Degradation of Materials in Nuclear Power Systems - Water Reactors, North Carolina, USA, 2013.
[17] M. Ahonen, S. Lindqvist, T. Sarikka, R. Mouginot, E. Leskelä, J. Lydman, U. Ehrnstén, P. Nevasmaa, T. Seppänen, P. Arffman, H. Hänninen, Thermal ageing and mechanical performance of narrow-gap dissimilar metal welds, VTT Technol. 333 (2018).
[18] P. Scott, P. Combrade, P. Ford, Environmentally-Assisted Degradation of Nickel-Base Alloys in LWRs, Advanced Nuclear Technology International, Mölnlycke, Sweden, 2011.
[19] E. Ibe, M. Sakagami, S. Uchida, Theoretical model analyses for effects of hydrogen injection on radiolysis of coolant water in BWR, J. Nucl. Sci. 23 (1) (1986) 11–28.
[20] P. Kelly, A. Jostsons, R. Blake, J. Napier, The determination of foil thickness by scanning transmission electron microscopy, Phys. Status Solidi (a) 31 (2) (1975) 771–780.
[21] Y. Seto, M. Ohtsuka, ReciPro: free and open-source multipurpose crystallographic software integrating a crystal model database and viewer, diffraction and microscopy simulators, and diffraction data analysis tools, J. Appl. Cryst. 55 (2022) 397–410.
[22] S. Jeng, Y. Chang, Microstructure and flow behavior of Ni–Cr–Fe welds with Nb and Mo additions, Materials Science Engineering A 560 (2013) 343–350.
[23] T. Wu, S. Jeng, J. Huang, The weld microstructure and mechanical properties of the Alloy 52 and its variants with applied electromagnetic stirring during welding, Metals 11 (2) (2021).

[24] Z. Zhang, Z. Yang, S. Lu, A. Harte, R. Morana, M. Preuss, Strain localisation and failure at twin-boundary complexions in nickel-based superalloys, Nat. Commun. 11 (4890) (2020).
[25] C. Brown and W. Mills, Load path effects on the fracture toughness of Alloy 82H and 52 welds in low temperature water, in Proceedings of the 12th International Symposium on Environmental Degradation of Materials in Nuclear Power Systems - Water Reactors, Salt Lake City, Utah, USA, 2005.
[26] M. Toloczko and S. Bruemmer, Crack growth response of Alloy 152 and 52 weld metals in simulated PWR primary water, in Proceedings of the 14th International Symposium on Environmental Degradation of Materials in Nuclear Power Systems - Water Reactors, Virginia, USA, 2009.
[27] H. Kim, M. Cho, G. Kim, Influence of hydrogen absorption on stacking fault of energy of a face-centered cubic high entropy alloy, Met. Mater. Int. 28 (2022) 2637–2645.
[28] J. Hermida, A. Roviglione, Stacking fault energy decrease in austenitic stainless steels induced by hydrogen pairs formation, Scr. Mater. 39 (8) (1998) 1145–1149.
[29] Z. Harris, S. Lawrence, D. Medlin, G. Guetard, J. Burns, B. Somerday, Elucidating the contribution of mobile hydrogen-deformation interactions to hydrogen-induced intergranular cracking in polycrystalline nickel, Acta Mater. 158 (2018) 180–192.
[30] H. Eom, J. Shin, B. Kong, C. Jeong, C. Jang, D. Ahn, D. Jang, Dissolution of nanosized NbC precipitates in austenite matrix during elastic deformation - Deleterious effect of high number density, Materials Science Engineering A 833 (142506) (2022).
[31] M. Martin, B. Somerday, R. Ritchie, P. Sofronis, I. Robertson, Hydrogen-induced intergranular failure in nickel revisited, Acta Mater. . 6 (7) (2012) 2739–2745.
[32] H. Shi, S. Nandy, H. Cheng, B. Sun, D. Ponge, In-situ investigation of the interaction between hydrogen and stacking faults in a bulk austenitic steel, Acta Mater. 262 (119441) (2024).
[33] P. Ferreira, I. Robertson, H. Birnbaum, Influence of Hydrogen on the Stacking-Fault Energy of an Austenitic Stainless Steel, Mater. Sci. Forum 207 (1996) 93–96.
[34] D. An, W. Krieger, S. Zaefferer, Unravelling the effect of hydrogen on microstructure evolution under low-cycle fatigue in a high-manganese austenitic TWIP steel, Int. J. Plast. 126 (102625) (2020).
[35] Y. Kong, P. Kathayat, A. Williamson, Influence of stacking fault energy and hydrogen on deformation mechanisms in high Mn austenitic steels during in-situ tensile testing, Int. J. Hydrog. Energy 148 (149833) (2025).
[36] H. Luo, Z. Li, D. Raabe, Hydrogen enhances strength and ductility of an equiatomic high-entropy alloy, Sci. Rep. 7 (9892) (2017).
[37] X. Zhou, C. Nowak, R. Skelton, An Fe–Ni–Cr–H interatomic potential and predictions of hydrogen-affected stacking fault energies in austenitic stainless steels, Int. J. Hydrog. Energy 47 (1) (2022) 651–665.
[38] C. Yu, T. Okita, T. Kawabata, The effects of alloying elements on hydrogen-affected generalized stacking fault energy and dislocation behavior in nickel-based alloys, Mater. Chem. Phys. 341 (130907) (2025).
[39] M. Koyama, T. Ogawa, D. Yan, Hydrogen desorption and cracking associated with martensitic transformation in Fe-Cr-Ni-Based austenitic steels with different carbon contents, Int. J. Hydrog. Energy 42 (42) (2017) 26423–26435.
[40] A. Ebner, E. Plesiutschnig, H. Clemens, R. Pippan, V. Maier-Kiener, Rate-depending plastic deformation behaviour in a nickel-base alloy under hydrogen influence, Int. J. Hydrog. Energy 46 (2021) 38132–38143.
[41] A. Barou, P. Joly, E. Andrieu, L. Laffont, C. Blanc, Hydrogen contribution to low temperature embrittlement during PWR exposure of an alloy 82 weld metal, Int. J. Hydrog. Energy (2024).
[42] E. Richey and G. Young, The effect of deaerated water on the toughness of nickel-based alloys, in Proceedings of the 15th International Symposium on Environmental Degradation of Materials in Nuclear Power Systems - Water Reactors, 2011.
[43] M. Ahonen, U. Ehrnstén, T. Saukkonen, O. Todoshchenko and H. Hänninen, Factors affecting low temperature crack propagation (LTCP) susceptibility of Nickel-based alloy 182, 82, 152 and 52 weld metals, in 17th International Conference on Environmental Degradation of Materials in Nuclear Power Systems – Water Reactors, Ottawa, Ontario, Canada, 2015.
[44] G. Lu, Y. Zhao, Z. Wen, T. Zhao, Y.W. W, Z. Yue, Temperature dependence of hydrogen embrittlement susceptibility of nickel-based single crystal superalloy, J. Alloy. Compd. 1020 (179505) (2025).
[45] Q. Peng, T. Shoji, J. Hou, Y. Takeda and T. Yonezawa, Environmental assisted crack growth in cold worked alloy 690 in primary water at low and high temperatures, in Proceedings of the 15th International Symposium on Environmental Degradation of Materials in Nuclear Power Systems - Water Reactors, 2011.
[46] K. Sakima, H. Suzuki and H. Fujiwara, Research and evaluation of low temperature crack propagation of Ni base alloys in actual plants, in Proceedings of the 15th International Symposium on Environmental Degradation of Materials in Nuclear Power Systems - Water Reactors, 2011.
[47] A. Fazi, P. Ferreirós, Y. Ge, S. Lu, M. Thuvander, Z. Que, Unexpected thermal aging effect on brittle fracture and elemental segregation in modern dissimilar metal weld, Mater. Charact. 217 (114419) (2024).
[48] Z. Que, T. Saario, A. Toivonen, U. Ehrnstén, Stress corrosion cracking initiation susceptibility of Alloy 182 with different surface treatments, Corros. Sci. 196 (110037) (2022).
[49] A. Vainionpää, P. Ferreirós, T. Seppänen, Z. Que, Microstructural insights into effects of pressurized water reactor environment and cyclic loading parameters on the low cycle fatigue behavior of 316L stainless steel, Int. J. Fatigue 198 (109016) (2025).
[50] U. Ehrnstén, P. Andresen, Z. Que, A review of stress corrosion cracking of austenitic stainless steels in PWR primary water, J. Nucl. Mater. 588 (154815) (2024).